Physics – Uspekhi **64** (7) 702 – 721 (2021)

REVIEWS OF TOPICAL PROBLEMS PACS numbers: 61.05.F –, 61.66.Dk, 64.60.Cn, **75.80.+q**

Neutron scattering in studies of Fe-based functional alloys (Fe – Ga, Fe – Al)

A M Balagurov, I S Golovin

DOI: https://doi.org/10.3367/UFNe.2020.11.038886

Contents

Abstract. Discovered in the early 2000s, giant magnetostriction prompted many experimental and theoretical studies. However, the physical mechanism underlying this important functional property has not been fully understood, despite 20 years of continuous effort. The models currently under discussion are based on the concept of specifically ordered microscopic regions that emerge in a disordered crystal matrix. Of special importance in detecting suchlike structural states are techniques that involve the scattering of X-ray (synchrotron), electron, and neutron radiation. The current state of structural studies of Fe – Ga and Fe – Al alloys is reviewed, with the focus on neutron diffraction.

Keywords: Fe – Ga and Fe – Al alloys, giant magnetostriction, atomic structure, phase transitions, neutron diffraction

1. Introduction

Iron-based alloys exhibit many functional properties that have been widely used in various technologies for a long time. One of them is giant magnetostriction, discovered in the early 2000s in Fe – Ga alloys and actively studied over the past 20 years. Classical magnetostriction — a change in the size of a body if its magnetic state changes or if it is exposed to an external magnetic field — is a well-studied physical phenomenon, a detailed description of which can be found in any textbook on magnetic phenomena in condensed media. Since the discovery of magnetostriction by J Joule in 1842, this phenomenon has been fully understood, its microscopic content determined, and a physical interpretation of it provided; it is now widely used in technology.

The situation with what is meant by the term 'giant magnetostriction' looks less clear. K P Belov et al. [1] published in 1983 in *Physics–Uspekhi* a review under this very title. It contained a detailed description of magnetostriction in rare earth metals (REMs) and some compounds based on REMs and actinides. The appearance of this review was associated with the discovery in the early 1960s of the enhanced magnetostriction of metallic terbium and dysprosium, which was at low temperatures ~ 100 times larger than that of iron. This phenomenon, which was explained using the model of interaction of an anisotropic electron cloud of f-electrons with the crystal field of the lattice, was named by Belov et al. 'giant magnetostriction.' However, the magnetostriction discovered much later in Fe – Ga alloys, which is approximately 20 times larger than that of magnetostriction of Fe, was also referred to as 'giant' (see, e.g., [2]), although the physical mechanisms of its formation seem to be completely different from those in the case of REMs.

It is noteworthy that a somewhat similar situation has developed in relation to the phenomenon of high magnetoresistance exhibited by multilayer heterostructures and perovskite-like manganese oxides. Both effects, whose physical nature is completely different, were initially designated as 'giant magnetoresistance.' However, to avoid confusion, the effect in manganese oxides was later referred to as 'colossal magnetoresistance.' The terminology for magnetostriction apparently also needs to be refined.

This has not yet been done, and giant magnetostriction is understood in this review as a phenomenon first found for Fe – xGa alloys, the magnetostriction constant $(3/2)\lambda_{100}$ of which in the range $x \approx 18-28$ at.% is $(250-400) \times 10^{-6}$ in poly- or single crystals, respectively [3]. This phenomenon, in

A M Balagurov [(1, *)], **I S Golovin** [(2, †)]
[(1)] Joint Institute for Nuclear Research,
ul. Joliot-Curie 6, 141980 Dubna, Moscow region, Russian Federation
[(2)] National University of Science and Technology MISIS,
Leninskii prosp. 4, 119049 Moscow, Russian Federation
Tel. +7 (49621) 68-844, +7 (495) 955-01-34
E-mail: [(*)] bala@nf.jinr.ru, [(†)] i.golovin@misis.ru

Received 21 June 2020, revised 23 November 2020
Uspekhi Fizicheskikh Nauk **191** (7) 738 – 759 (2021)
Translated by M Zh Shmatikov

contrast to REMs, is observed at room temperature and, despite the fact that the magnetostriction of Fe–xGa alloys is several times smaller than that in REMs, it was acknowledged as a landmark for the materials science of magnetostrictive materials and initiated a plethora of studies in this area. However, despite almost 20 years of effort, the mechanisms of the formation of giant magnetostriction in Fe–Ga alloys remain unclear. No clear answer has been provided as yet for several fundamental issues regarding the mechanism of the crucial effect of nonmagnetic Ga on magnetostriction, the emergence of two maxima in the magnetostriction constant at 17–19 and 26–27 at.% of gallium content, and the growth of the magnetostriction constant if a small amount (less than 0.1%) of rare earth elements are added to the Fe–Ga alloy. This list also includes the question of why the dependence of magnetostriction on x in Fe–xAl alloys is almost the same as in Fe–xGa and has a maximum at x in the region of about 18 at.%, but the second maximum is absent.

The models of giant magnetostriction currently under discussion are based on the concept of a disordered (from the point of view of the arrangement of Fe and Ga atoms) crystalline matrix, within which microscopic regions containing Ga and REM atoms (La, Tb, etc.) ordered in a specific way emerge. An alternative approach is possible in some cases: namely, it may be assumed that the long-range crystalline order of the matrix is violated due to the emergence in it of microscopic regions that are ordered but in a different way.

It should be noted that thermodynamically equilibrium inhomogeneous states have long been recognized as an indispensable attribute of the formation of many unusual physical properties of crystals, including high-temperature superconductivity and the already mentioned colossal magnetoresistance of manganites. Examples of discovered inhomogeneous states in superconductors are charge-separated regions with characteristic dimensions $L \sim 20$ Å, which are formed at the electronic level, and coexisting mesoscopic dielectric and superconducting regions with different contents of superstoichiometric oxygen ($L \sim 1000$ Å) in $La_2CuO_{4+\delta}$. Both of these types of inhomogeneous states ('electronic' and 'chemical') are discussed in detail in review [4], in which phase separation is identified as the common cause of their appearance. An inhomogeneous state is observed in manganites in the form of an equilibrium mesoscopic ($L \sim 500-2000$ Å) stratification into ferromagnetic-metallic and antiferromagnetic-dielectric phases, the formation of magnetic polarons being possible in the antiferromagnetic regions [5]. The assumption that inhomogeneous states of Fe–Ga and Fe–Al alloys are a possible reason for the formation in them of enhanced magnetostriction values may be recognized, based on an analogy, as a correct avenue for the ongoing search for models.

A special role in the diagnostics of inhomogeneous states of crystals belongs to methods that involve the scattering of X-ray, synchrotron, electron, and neutron short-wave radiation. It is these techniques that enabled obtainment of the information necessary for the development of physically justified models regarding both the atomic structure of a material and the organization of its submicroscopic structure, i.e., atomic level microstructures. Another important area of issues related to constructing the models that can be studied using these methods is the occurrence of structural phase transitions in ordered alloys with a change in temperature and the formation of certain structural phases under various conditions of alloy preparation and subsequent heat treatment, since phases differ by their magnetostriction constants, up to a difference in sign.

This review discusses the current situation with structural studies of ordered iron-based alloys with an emphasis on the use of neutron diffraction. Basic information on giant magnetostriction is presented, and information on the structural phase states of Fe–Ga and Fe–Al alloys and phase transitions in them is systematically expounded. The main focus is on Fe–xGa alloys, especially the wide range of gallium content, up to $x \approx 30$ at.%. The Fe–xAl alloys are considered primarily in what regards the similarities and differences between their structural behaviors as a function of x compared with Fe–xGa alloys. The specific features of the microstructure of alloys are discussed on the basis of electron microscopic and diffraction studies performed recently. There are also relatively short sections on new data on the kinetics of phase transitions in Fe–Ga alloys and on the relationship of the processes of ordering the structure with the crystal lattice. The material-science properties of alloys are omitted, since they are discussed in detail in our recent review [6].

The structural states are presented in this review in accordance with the 'Strukturbericht designation,' notations adopted in crystallography and materials science. A description of all the structural phases mentioned in the review can be found in the appendix 'Crystal Structure Descriptions' in reference book [7], which contains images of the structure, chemical formulas, Strukturbericht symbols, space groups, etc. The notations of the composition of alloys also include the atomic percentage of the 2nd, 3rd, etc. components, which is also accepted in materials science. It is easy to determine that, for example, a compound with the chemical formula $Fe_{3-\alpha}Ga_{1+\alpha}$ is an Fe–xGa composition, where $x = 100(1+\alpha)/4$ at.%. The designation 'at.%' next to x is omitted below for brevity. Also, for the convenience of comparing the diffraction spectra of the phases derived from the body-centered cubic (bcc) structure (A2, B2, and $D0_3$), a unified system of Miller indices reduced to the cell of the $D0_3$ phase is used.

2. Magnetostriction and structural states of Fe–Ga and Fe–Al alloys

The phenomenon of magnetostriction consists of a change in the linear dimensions of a crystalline material and, in some cases, in its volume when magnetization of the material changes. A distinction is made between spontaneous and induced magnetostriction: the former occurs during the transition from the para- to the ferromagnetic (FM) state in the absence of an external magnetic field, while the latter emerges if a magnetic field is applied. Magnetostriction in a single crystal is usually anisotropic, and to describe it, dimensionless magnetostrictive constants in some directions are introduced. For example, in the case of crystals with cubic symmetry, these are usually λ_{100} and λ_{111}, which characterize the relative changes in the edge lengths and the body diagonal of the cube. It is customary to report the values $\lambda_1 = (3/2)\lambda_{100}$ and $\lambda_2 = (3/2)\lambda_{111}$, which are the coefficients in the expansion of magnetostriction along the components of the magnetization vectors and the direction of measurement. For a polycrystalline material, averaging is carried out over different crystallographic directions, and the value of λ_S is presented, which is the magnetostriction constant when the magnetization reaches saturation.

It follows from the most general considerations based on the Curie symmetry principle that the emergence of spontaneous magnetization in an FM crystal below the Curie temperature, T_C, and, consequently, magnetostriction, should be accompanied by a change in the symmetry of the crystal. If magnetization arises in the [100] direction of a cubic crystal belonging to the class $m3m$, the crystal symmetry should decrease to tetragonal $(4/mmm)$. However, spontaneous magnetostriction is usually very small and, for example, it is generally believed that the symmetry of α-Fe at room temperature is cubic, despite FM ordering.

The anisotropy of magnetostriction arises due to two main physical mechanisms: the already mentioned interaction of the anisotropic electron cloud with the field of the crystal lattice and the dipole interaction between the magnetic moments of electrons. The first of these mechanisms is of importance primarily for materials that contain rare earth elements, while the second, for materials based on 3d metals. An isotropic contribution is also distinguished, which arises due to the modification of exchange interactions with a change in the magnetization of the material. A detailed presentation of knowledge about the magnetostriction of ferromagnets can be found in both monographs and textbooks, for example, in [8, 9].

The first detailed study of the magnetic properties of Fe–Ga alloys in a gallium concentration range of 15–30% was carried out in the early 1970s [10]. In particular, it was determined in this work that the magnetic moments of iron in two possible ordered phases $D0_3$ and $L1_2$ are $2.05\,\mu_B$ and $2.39\,\mu_B$, respectively. However, interest in these alloys only surged 30 years later after the publication of two studies by Clark et al. [11, 12]. The main result of Ref. [11] was the discovery of a tenfold increase in magnetostriction in the Fe–17Ga compound in comparison with pure iron. It was found that $(3/2)\lambda_{100} \approx 311 \times 10^{-6}$ (311 ppm) in Fe–17Ga, while the same value for α-Fe is about 30 ppm. Magnetostriction was measured in the next study by Clark [12] on Fe–xGa single crystals for a wide range of concentrations, $4 \leqslant x \leqslant 27$. The now famous dependence of $(3/2)\lambda_{100}$ on x with two maxima at $x \approx 18$ and $x \approx 26$ was discovered. The measurements were carried out for two types of samples: quenched from 1000 °C in water and slowly cooled from the same temperature in a furnace at a rate of $\sim 10\,^\circ\mathrm{C\ min^{-1}}$. The magnetostriction in quenched samples turned out to be slightly larger (by 15–25%), although, in general, its behavior in both types of the samples was similar. A significant change in magnetostriction depending on the prehistory of the sample (quenching, annealing) naturally suggested that its occurrence is somehow related to the formation of inhomogeneities (the appearance of ordered regions) of the structure. It was mentioned in these first studies by Clark et al. that the magnetostriction of Fe–xAl also has a maximum at $x \approx 15$–20 at the $(3/2)\lambda_{100} \approx 150$ ppm level, as was found as early as the late 1950s [13].

These results were refined and extended in subsequent studies by various authors; they were presented (Fig. 1) in the first review on this topic [3] in comparison with data on Fe–xAl and Fe–xGa with additions of third elements (Ni, Co, Sn, Si, Ge, etc.), which, as it turned out, decrease to some extent the magnetostriction constant. It was asserted in [3] that the critical issue for understanding the unusual behavior of Fe–xGa alloys is the identification of structural phases and phase transformations when varying the gallium content. Attention was also drawn to the significant differences

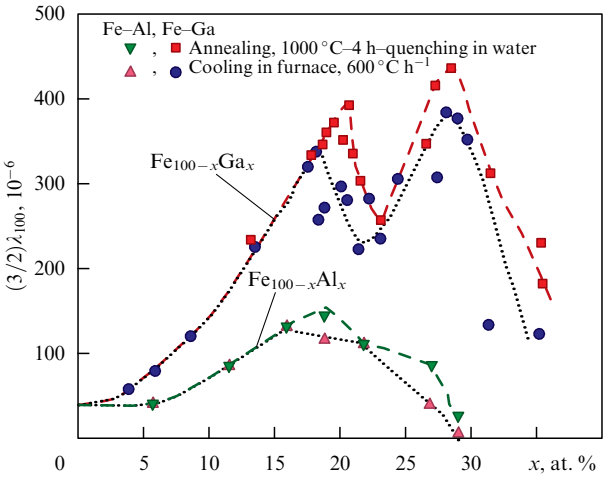

Figure 1. (Color online.) Magnetostriction constant $(3/2)\lambda_{100}$ for Fe–xAl and Fe–xGa single crystals as a function of x. The measurements were carried out on samples heated to the temperature of the transition to the disordered A2 phase and cooled in a furnace at a rate of $10\,^\circ\mathrm{C\ min^{-1}}$ (blue dots and red triangles) or quenched in water (red squares and green triangles). (Figure adapted from [3].)

between the equilibrium [14] and metastable [15] Fe–Ga phase diagrams. One of the main conclusions done in review [3] is the hypothesis that stabilization of the inhomogeneous structure is a key factor in enhancing the magnetostriction of Fe–Ga alloys. It was this assumption that was used later as the basis for the development of numerous microscopic models.

The types of structures observed in the compositions Fe–xAl and Fe–xGa, depending on x and the temperature prehistory, are largely similar, although Fe–xGa exhibits greater diversity of these types due to the emergence in certain temperature-concentration regions of close-packed ordered phases based on A1- and A3-lattices, namely the $L1_2$ and $D0_{19}$ structures. To avoid misunderstanding, considered everywhere below will be the properties of samples after casting (*as cast* state), unless otherwise stated. It is clear that this state is metastable (nonequilibrium) and depends on the ingot cooling rate. Both alloys have up to $x \approx 19$ a bcc disordered α-Fe structure. A partially ordered $D0_3$ phase emerges at larger x, which exists up to $x \approx 30$ in Fe–xGa and up to $x \approx 35$ in Fe–xAl. The $D0_3$ phase can be completely ordered (up to thermal fluctuations) in the composition with $x = 25$ alone, which corresponds to the $Fe_3Ga(Al)$ structure. A partially ordered B2 phase is also formed with a further increase in x, the total order in which can only exist in the composition with $x = 50$. The fully ordered B2 phase is indeed found in Fe–50Al, whereas in Fe–xGa, more complex phases emerge even at $x > 35$, whose structure is still a subject for discussion. Recent efforts have made it possible to understand the structure of the $Fe_{13}Ga_9$ (Fe–41Ga) intermetallic compound, the atomic structure of which was determined from X-ray data and confirmed later by neutron diffraction data and calculations based on the density functional theory [16], while the structure of the β-phase of the Fe_6Ga_5 (Fe–45Ga) intermetallic compound and its evolution in the process of heating to high temperatures and subsequent cooling were refined in [17].

No other phases, except for A2, $D0_3$, and B2, have been found in the compositions Fe–xAl in the range $0 \leqslant x \leqslant 50$, including cases where they are heated up to melting. The

Table. Main characteristics of the structural phases observed in Fe–xGa and Fe–xAl alloys. The columns show the symmetry of the crystal lattice, space group, unit cell parameters, number of atoms in the cell (N), and atomic volume (V_a) (the volume of the unit cell per atom) for Fe–Ga. The values of cell parameters are approximate since they depend on compositions and the temperature of measurement.

Phase	Symmetry	Space group	Fe–Ga	Fe–Al	N	V_a, Å^3
A1	Cubic	$Fm3m$	$a \approx 3.72$ Å		4	12.87
A2	Cubic	$Im3m$	$a \approx 2.90$ Å	$a \approx 2.90$ Å	2	12.19
A3	Hexagonal	$P6_3/mmc$	$a \approx 2.64$ Å $c \approx 4.28$ Å		2	12.92
B2	Cubic	$Pm3m$	$a \approx 2.92$ Å	$a \approx 2.93$ Å	2	12.45
$D0_3$	Cubic	$Fm3m$	$a \approx 5.81$ Å	$a \approx 5.79$ Å	16	12.14
$D0_{19}$	Hexagonal	$P6_3/mmc$	$a \approx 5.29$ Å $c \approx 4.28$ Å		8	12.92
$L1_2$	Cubic	$Pm3m$	$a \approx 3.72$ Å		4	12.87

situation in Fe–xGa compositions up to $x \approx 24$ is the same as in Fe–xAl; however, in the range $24 \leqslant x \leqslant 30$, after slow cooling from 900 °C to room temperature, a mixture of $D0_3$, $L1_2$, and $D0_{19}$ phases emerges in the proportions that depend on x and on the cooling rate. The phases $L1_2$ and $D0_{19}$ are partially ordered; complete order is also possible in them only at $x = 25$. The destruction of the order leads to the transitions $L1_2 \rightarrow$ A1 and $D0_{19} \rightarrow$ A3, where A1 is a face-centered close-packed cubic (fcc) structure and A3 is a hexagonal close-packed structure. The main structural characteristics of these phases are listed in the table, and the distribution of atoms over crystallographic positions can be found in [18].

Three more versions of ordered structures are mentioned in studies of Fe–Ga alloys: namely $D0_{22}$, m-$D0_3$, and $L6_0$. These structures are not present in any of the published Fe–Ga phase diagrams, but signs of their existence in the form of locally ordered regions were found in a number of experiments using electron diffraction (this issue is considered in more detail in Section 4). The $D0_{22}$ structure is body-centered tetragonal, space group $I4/mmm$, $a \approx 3.70$ Å, $c \approx 7.20$ Å, 8 atoms per cell, $V_a \approx 12.32$ Å^3. Considered in [2] as a precursor of the $L1_2$ phase in the $D0_3 \rightarrow L1_2$ transition, it has the same atomic pattern as $L1_2$ (the $L1_2$ cell doubled along the c-axis). The modified $D0_3$ (m-$D0_3$) structure that repeats the $D0_3$ structure, but with the positions of the pair of Fe and Ga atoms swapped, is not independent, since it can be transformed into $L6_0$ by changing the coordinate system, i.e., in fact, m-$D0_3$ and $L6_0$ represent the same structure. Nevertheless, some authors prefer using m-$D0_3$ because it is more convenient for comparing with $D0_3$. The $L6_0$ structure is face-centered tetragonal (fct), the space group is $P4/mmm$, $a \approx a(D0_3)/\sqrt{2} \approx 4.10$ Å, $c \approx a(D0_3)/2 \approx 2.98$ Å, 4 atoms per cell, $V_a \approx 12.52$ Å^3.

Evidence of yet another nonstandard type of ordering was found in the study of a Fe–26.9Ga single crystal using a synchrotron radiation beam [19]. Continuous scanning of a large volume of reciprocal space enabled the observation of many reflexes ($\sim 90\%$ of the total number), the presence of which could be explained by assuming a tripled cubic cell of the $D0_3$ phase. It turned out in the course of the further search for their optimal description that they correspond to the hexagonal lattice with $a \approx \sqrt{8}a_0$ and $c \approx \sqrt{12}a_0$, where $a_0 = 0.287$ nm is the lattice parameter of α-Fe. None of the previously described superstructures derived from the bcc lattice coincides in metric with the discovered hexagonal cell. Unfortunately, a structural analysis of this phase turned out to be impossible due to the twinning of the single crystal and the complete overlap of the entire families of reflexes with the peaks of the $D0_3$ phase.

The presented data on the boundaries of the existence or emergence of certain phases should be considered as conventional for several reasons. First, they depend on the cooling rate of the alloy and, to some extent, on the dimensions of the ingot, since cooling occurs at different rates on the surface and in the bulk of the ingot. A detailed analysis of the so-called TTT diagram (Time–Temperature–Transformation) for the Fe–27Ga composition, which reflects the correlation between the cooling rate and the temperature of the appearance and decomposition of structural phases in this composition, is presented in [20]. This study found, in particular, two critical cooling rates that relate to the beginning and completion of the appearance of the equilibrium $L1_2$ phase from the metastable A2 or $D0_3$ phases. A more basic reason for the uncertainties is the already mentioned possible formation in a disordered matrix of structurally ordered regions with a wide range of characteristic sizes. A cluster structure is formed, and a particular sample should be assigned then according to some criteria to the A2 phase, while, according to other criteria, to the $D0_3$ phase.

The magnetic and magnetostrictive properties of various structural phases differ significantly. Both main ordered phases $D0_3$ and $L1_2$ of compositions Fe–xGa with $x \approx 27$ are ferromagnetic at room temperature, but have different Curie temperatures and different magnitudes and signs of magnetostriction. For example, the magnetostriction constant is $\lambda_S \approx 100$ ppm for polycrystalline Fe–27.8Ga if the sample is in the 100% $D0_3$ state but is $\lambda_S \approx -50$ ppm for 100% $L1_2$. Consequently, a sample with virtually zero magnetostriction can be obtained by controlling in some way the ratio of these phases [21, 22].

3. Neutron scattering in alloy research

There are naturally a large number of standard (metallurgical, physicochemical, etc.) experimental methods to analyze the physical properties and microstructure of alloys. However, it is apparent that, to determine the nature of the high magnetostriction of Fe–Ga alloys, it is necessary to use state-of-the-art structural methods. They include transmission and scanning electron microscopy, X-ray or synchrotron radiation diffraction, and scattering of slow neutrons. It is the use of these methods that made it possible to obtain comprehensive information about the atomic structure of ordered alloys and the arrangement of their microstructure, to reveal the

structural features in the bulk and on the surface of the sample, to analyze phase transitions during various thermal operations, etc.

The atomic structure of all the phases listed in the table is very simple, since the atoms are located in particular positions, and only the unit cell parameters, position occupancy factors, and (sometimes) the thermal factors of atoms are subject to refinement in the course of structural analysis. Information about the atomic structure that can be obtained by the methods mentioned above is often complementary, since none of them is universal. The fundamental reason for this is the essential differences among the interaction of electrons, X-ray (synchrotron) radiation, or neutrons with matter. It is of no less importance that the subjects of research should be prepared for each of these methods in a completely different way. Practice shows that, in general, the employment of modern structural methods, especially if combined with each other, makes it possible to obtain quite objective information about the atomic structure of alloys.

The situation with studies of the submicroscopic structure of alloys, which is customarily understood as any deviations in the arrangement of atoms from the ideal long-range crystalline order, is much more complicated. The usual characteristics, such as the level and anisotropy of microstresses in grains, the extent to which crystallographic texture is pronounced, the density of defects, and the characteristic sizes of coherently scattering domains (CSDs), are determined reliably. However, problems are usually encountered in relation to the attribute of utmost importance for alloys with giant magnetostriction: the morphology of regions with an ordered arrangement of atoms and the degree of ordering in them. Nevertheless, there is some progress in studying the submicroscopic structure of alloys (briefly referred to below as the microstructure), and the information obtained is discussed in the subsequent sections.

The basics of transmission electron microscopy, both standard and high resolution (TEM and HRTEM), X-ray diffraction (XRD), synchrotron (SXRD), and neutron radiation (ND) are well known and have been extensively and in detail expounded on in the literature [23–25]. Consequently, only characteristic features of these methods and their advantages and limitations as applied to the study of metal alloys are briefly considered here.

The interaction of electrons with matter is determined by the electrostatic potential of atoms, which consists of the potential of nuclei and electrons. X-ray and synchrotron radiation is actually scattered only by the electrons of the atoms. Neutrons interact with the nuclei of atoms (strong or nuclear interaction) and the effective magnetic moment of the electrons of the atom (magnetic dipole interaction). The physical principles that govern the formation of the diffraction pattern of a crystal are the same for any type of radiation, and the specific features of the interaction are manifested primarily in the scattering cross section and, consequently, in the intensity of the diffraction maxima. All other things being equal, it can be estimated — adopting the average intensity of X-ray diffraction as a unit — that this figure for electrons will be $\sim 10^6$, for SXRD, about 10^2, and for neutrons, about 10^{-2}. If the completely different degree of absorption of these various kinds of radiation in the matter is also taken into account, it turns out that the characteristic thicknesses of the layer of the substance used to form the diffraction pattern are $(10^{-5}-10^{-6})$, $(10^{-3}-5\times10^{-2})$, and $(0.1-0.5)$ cm for electrons, X-rays, and neutrons, respectively. This determines the well-known features in the preparation of samples for analysis and the setup of the diffraction experiment (for more details, see textbook [26]). It may be asserted with some simplification that electron microscopy makes it possible to analyze the local structure, X-ray diffraction, the surface structure, and neutron diffraction, the bulk structure of alloys.

The penetration depth of synchrotron radiation can be significantly increased by choosing a small (down to $\lambda \sim 0.15$ Å) wavelength. The diffraction pattern can be recorded in this case in transmission, i.e., information about the bulk structure can be obtained. However, a very unfavorable consequence of such a short wavelength is the need to operate at small Bragg angles, which leads to a sharp increase in the geometric contribution to the width of the diffraction peaks. The inherent high resolution of SXRD deteriorates as a result and can be significantly inferior to the resolution of a neutron diffractometer. As for the measured intensities, it follows from the above figures that neutron diffraction is very much inferior to other diffraction methods. However, due to the significantly larger irradiated sample volume, the actual difference is not so catastrophic. As shown below, an advanced neutron diffractometer can scan the entire diffraction spectrum in a time of the order of one minute, and sometimes even faster, which is usually sufficient for studying phase transformations *in situ* and in real time.

In studying the structure and microstructure of alloys, the efficiency of neutron diffraction is primarily determined by three circumstances: the capacity to distinguish elements closely located in the periodic table, a large penetration depth, and a large cross section of the neutron beam. The last two points make it possible to avoid uncertainties associated with the coarse-crystalline and inhomogeneous structure of alloys and surface effects. For example, the typical dimensions of a synchrotron beam on a sample are 0.15×0.15 mm, and in some cases as low as 0.05×0.05 mm; one single crystal can be irradiated in this case with some contribution from neighboring single-crystal grains, and Debye–Scherrer rings look like a collection of individual spots. The neutron beam size ranges from one to several centimeters, and the extent of averaging over grain orientations may be very high. The unique ability of neutrons to respond to the magnetic structure of the material in the case of ferromagnetic alloys is not of utmost importance. This is due to the fact that magnetic scattering is only added for the FM state to the regular (nuclear) intensities of neutron diffraction peaks. Since the ordered magnetic moment of iron is $\sim 2\mu_B$ or less, this contribution is not large, and it is difficult to distinguish it against the background of very strong nuclear scattering. It is easier and more reliable as a result to determine the magnetic moment and, in general, the magnetic properties of samples by measuring their magnetization and magnetic susceptibility.

A disadvantage of this method in comparison with other diffraction techniques is the low intensity (luminosity) and possible activation of the samples. After even a short exposure to a neutron beam, the sample must often be kept for several days or even weeks for the induced activity to vanish.

The scattering of slow neutrons is usually characterized by the coherent scattering length b, which for most isotopes is a constant independent of the neutron energy (their values are given, for example, in Ref. [27]). These quantities for the elements mentioned in this review are $b_{Fe} = 9.45$, $b_{Ga} = 7.29$,

$b_{Al} = 3.45$, and $b_{Cr} = 3.64$ (in Fermi units; 1 fm $= 10^{-13}$ cm). It is seen that these values are significantly different, and they provide the necessary contrast for determining the characteristics of ordered alloys. We now show this by the example of the Fe–xAl alloy, which is in the ordered phases $D0_3$ or B2. The diffraction peaks of the $D0_3$ phase can be divided into two groups due to the ordering of the atomic structure: fundamental and superstructure. The peaks of the first group do not change their intensity when the ordering disappears, i.e., in the transition $D0_3 \rightarrow A2$, while the peaks of the second group vanish at this transition. The exclusion rules in the $D0_3$ phase are such that the sum of the Miller indices of the fundamental peaks must satisfy the condition $h + k + l = 4n$ (for example, 220, 400, etc.); all other peaks are superstructure ones (for example, 111, 200, 311, etc.). The following formulas are valid for the temperature dependences of the intensities of these groups (fundamental/superstructure) of peaks:

$$I_F(T) \sim V_F(T)\left|F_F(hkl)\right|^2 \exp\left[-W(T)\right], \qquad (1)$$
$$I_S(T) \sim V_S(T)\xi^2(T)\left|F_S(hkl)\right|^2 \exp\left[-W(T)\right],$$

where V_F and V_S are the sample volume and the volume occupied by the ordered phase ($V_S \leqslant V_F$), F_F and F_S are structural factors, ξ is the degree of ordering ($0 \leqslant \xi \leqslant 1$), and $\exp(-W)$ is the Debye–Waller factor. The structural factors of the fundamental and superstructure peaks for the stoichiometric composition Fe–25Al (Fe_3Al) are $F_F = 3b_{Fe} + b_{Al}$, $F_S = b_{Fe} - b_{Al}$. Substituting the coherent scattering lengths and assuming that ordering is complete ($\xi = 1$) and the entire sample volume is in an ordered state, we obtain for the peak intensity ratio $I_S/I_F \approx 0.04$, all other factors being equal.

Peaks with odd Miller indices (defined in the $D0_3$ phase cell), i.e., 111, 311, etc., are forbidden in the B2 phase, but superstructure peaks like 200, 222, etc. are allowed. For this structure, $F_F = b_{Fe} + b_{Al}$, $F_S = b_{Fe} - b_{Al}$, and we have for the intensity ratio $I_S/I_F \approx 0.22$. The difference between the scattering lengths of Fe and Ga is not as great as for Fe and Al, and similar numbers for the Fe–xGa compositions are: $I_S/I_F \approx 0.004$ for $D0_3$ and $I_S/I_F \approx 0.13$ for B2, i.e., superstructure peaks will be about 10 and 2 times weaker than those in Fe–xAl.

To find the actual ratios of intensity in the case of diffraction on a polycrystal, it is also necessary to take into account the multiplicity and Lorentz factors for specific peaks; in addition, the intensities can be distorted by the effect of texture, and the degree of ordering may be incomplete, but these numbers correctly represent the order of magnitude. The form of neutron diffraction spectra of compositions Fe–xAl in the $D0_3$, B2, and A2 phases is displayed in Fig. 2. It can be seen, in particular, that the intensities of superstructure peaks (111, 200, 311, 222, etc.) are high enough to be reliably detected.

It is this feature that was noted as one of the main advantages of neutron diffraction in studies of alloys in the pioneering study, which became classical, of this issue by K Shull, the future Nobel Prize winner [28]. Alloys have subsequently been actively studied by neutron scattering methods (diffraction, small-angle scattering, and inelastic scattering) in virtually all of the world's neutron research centers. The exploration focused on ordering effects, the structure of alloys with light impurities (hydrogen, oxygen, nitrogen), specific features of the magnetic structure, changes in the structure under radiation exposure, etc. These studies

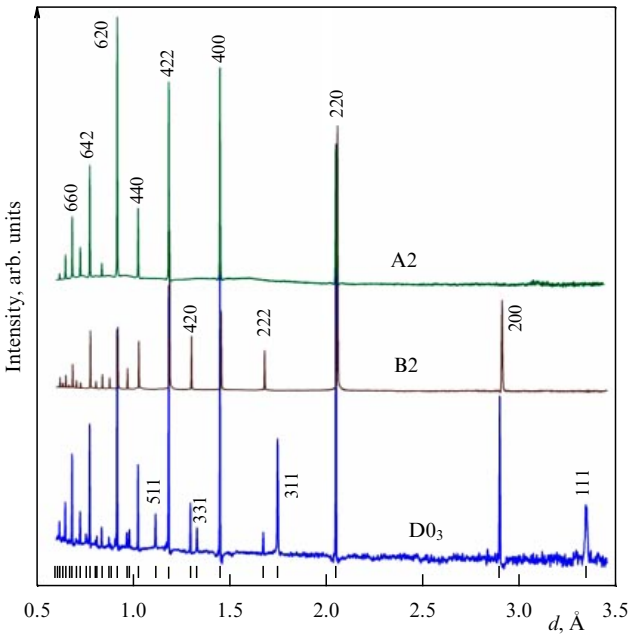

Figure 2. Neutron diffraction spectra of Fe–xAl compositions in the phases $D0_3$ ($x = 27$), B2 ($x = 50$), and A2 ($x = 16$). Vertical dashes show the calculated positions of the peaks in the $D0_3$ phase. Miller indices shown next to peaks are given for the $D0_3$ phase cell. The indices of the fundamental peaks are displayed on the graph for A2, and those for superstructure ones, on the graphs for B2 and $D0_3$.

are naturally ongoing at present, although the situation with neutron research in the world does not seem to be favorable. The problem is that stationary nuclear reactors, a large number of which were built in the 1960s–1970s, have exhausted their service life and their operations have been halted. For example, five major research reactors have been closed in Europe alone in the last decade. Experiments are also being carried out on pulsed neutron sources, but there are still too few of them (there were only six sources worldwide in 2020). Especially interesting results in the study of alloys using neutrons were obtained in Russia by V A Somenkov et al. at the Moscow-based reactor operated by the Research Center Kurchatov Institute (see the "Metal hydrides as solid solutions" section in monograph [25]) and by B N Goshchitskii's laboratory (Mikheev Institute of Metal Physics, Ural Branch of the Russian Academy of Sciences, Ekaterinburg), where the structure of structural reactor steels was studied. Neutron research of alloys has been actively carried out since 2015 at the Frank Laboratory of Neutron Physics of the Dubna-based Joint Institute for Nuclear Research (JINR) at the IBR-2 pulsed reactor. Detailed information on research neutron sources in Russia and in the world and an analysis of the European strategy for their development can be found in review [29].

Most examples of neutron diffraction studies of Fe–xGa and Fe–xAl alloys discussed in this review are taken from the work performed on a high-resolution Fourier diffractometer (HRFD) operating at the IBR-2 reactor at JINR (Dubna) [30]. The HRFD is a time-of-flight diffractometer (TOF diffractometer). Consequently, backscatter detectors ($2\theta = 152°$) installed on it concurrently measure the spectrum in the d_{hkl} range to 4.5 Å, which is sufficient to detect peaks with the largest interplanar distances. The feature of the HRFD of importance for studying alloys is its capacity to switch between modes of high ($\Delta d/d \approx 0.0015$) and medium

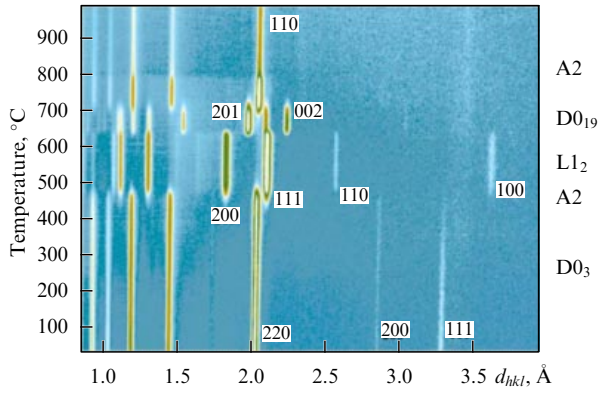

Figure 3. Diffraction spectra of the Fe–27Ga composition upon continuous heating at a constant rate of 2 °C min^{-1} from room temperature to 950 °C. The temperature–time axis runs from bottom to top, and the axis of interplanar distances, from left to right. The initial state is the $D0_3$ phase, for which superstructure peaks 111 and 200 and fundamental peak 220 are indicated. Then, the $D0_3 \rightarrow$ A2 transition occurs, and phases $L1_2$ (peaks 100, 110, 111, and 200), $D0_{19}$ (peaks 002 and 201), and A2 (peak 110) sequentially emerge. The spectra were measured every minute; the heating time was about 450 min, i.e., the diagram contains about 450 separate diffraction spectra. (Figure taken from [18].)

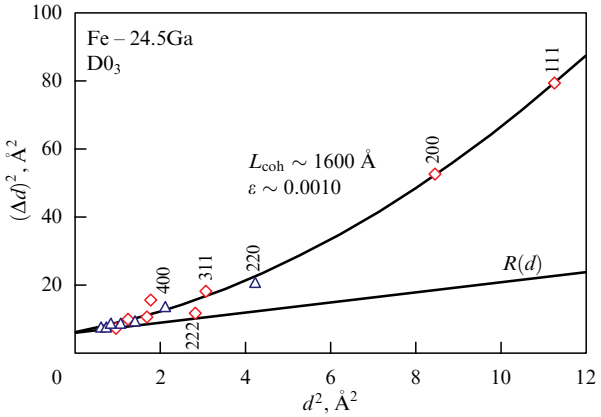

Figure 4. Williamson–Hall construction for the width of the diffraction peaks of the composition Fe–24.5Ga, which is in the $D0_3$ phase. All experimental points (fundamental peaks are shown with triangles, superstructure ones, with diamonds) fall on a parabolic dependence that corresponds to $\varepsilon \sim 0.001$ and $L_{coh} \sim 1600$ Å. Miller indices are indicated for some peaks. Displayed below is the linear dependence for the HRFD resolution function measured on a standard Al_2O_3 sample. The (Δd) values are multiplied by 10^3.

$(\Delta d/d \approx 0.015)$ resolution, the intensity in the latter case being significantly ($\sim$ 10 times) higher. The first mode is used to analyze structural and microstructural characteristics, while the second one is intended to detect weak superstructure peaks and perform *in situ* studies of phase transformations (examples of both types of neutron diffraction spectra are presented for Fe–27Ga in [18]). For parallelepiped-shaped alloy samples with standard dimensions of $4 \times 8 \times 50$ mm, an HRFD operating in the medium resolution mode needs only 1 min to measure the complete diffraction spectrum (measurements were carried out in some cases with a time resolution of 1 s [31]). This performance is usually sufficient for studying transient processes in alloys. This can be seen from Fig. 3, which shows how phase transformations exhibit themselves in the diffraction spectra measured upon heating at a constant rate the Fe–27Ga composition to 950 °C. The disappearance of some superstructure peaks and the emergence of other peaks make it possible to reliably trace the occurring sequence of transitions: $D0_3 \rightarrow A2 + L1_2 \rightarrow L1_2 \rightarrow D0_{19} \rightarrow A2$.

Another important feature of the HRFD is the very simple dependence of its resolution on the interplanar spacing, namely $(\Delta d)^2 \approx C_1 + C_2 d^2$, where Δd is the total width of the diffraction peaks (FWHM), C_1 and C_2 are some constants determined in the experiment with a standard sample. An additional contribution to the peak width arises in the case of a real crystal in accordance with the Williamson–Hall analysis (see, e.g., [32]) due to the effect of microstresses, ε, and the finite size of the coherently scattering domains, L_{coh}. This contribution is described on the scale of interplanar distances by the formula $(\Delta d)^2 = (2\varepsilon)^2 d^2 + (k/L_{coh})^2 d^4$, if the Gaussian approximation is used for the distribution functions (k is a dimensionless factor close to unity that takes into account the shape of the coherently scattering domain (CSD)). Combining both expressions, we obtain the following formula for the dependence of the widths of the diffraction peaks of a real crystal on the interplanar distance:

$$(\Delta d)^2 = C_1 + (C_2 + C_3) d^2 + C_4 d^4 , \qquad (2)$$

where $C_3 \approx (2\varepsilon)^2$ and $C_4 \approx (k/L_{coh})^2$. If the size effect is negligible (large CSD), the dependence $(\Delta d)^2$ on d^2 is linear; otherwise, it is parabolic. Consequently, by plotting these dependences in a sufficiently large interval of d_{hkl}, ε and L_{coh} can be found (Fig. 4). Experience operating the HRFD shows that its resolution makes it possible to confidently determine microstresses in crystallites at the level of $\varepsilon \approx 0.001$ or more and characteristic sizes of the CSD at the level of $L_{coh} \approx$ 3000 Å or less. If the CSD size significantly decreases (to 50 Å or less), diffraction (Bragg) scattering smoothly transforms into diffuse scattering, the peaks are substantially broadened, and special efforts are needed to separate them from the background.

4. Specific features of the microstructure of Fe–Al and Fe–Ga alloys

It was noted in the Introduction that the currently discussed models of giant magnetostriction in Fe–Ga alloys are based on the assumption that local ordering occurs in a disordered crystal matrix, i.e., the matrix with a statistical population of the crystallographic positions of the atoms that constitute the alloy. Indeed, much evidence of the specific organization of the microstructure of these alloys has been obtained using microscopic research methods (HRTEM, XRD, SXRD, and ND). If Fe–Ga alloys without additions of rare-earth metals (La, Tb, etc.) are considered, this evidence can be divided to a first approximation into two groups. The first one includes data on the bulk phase inhomogeneity of a material that consists of nanoscale precipitates (clusters) of one of the standard ordered phases in a disordered or less ordered matrix. This conclusion is based on an analysis of the characteristics of superstructure diffraction peaks and diffuse scattering. The second group contains evidence of the formation of tetragonal ordered phases that are nonstandard for Fe–Ga, such as m-$D0_3$, $L6_0$, and $D0_{22}$, which are primarily obtained by the TEM and HRTEM methods. We now examine this evidence in more detail.

It is well known that the formation of long-range order regions in alloys strongly depends on the specific composition and conditions of alloy preparation and its subsequent heat

treatment. It is usually believed that this formation leads to a microstructure that consists of antiphase domains (APDs) or clusters of relatively small sizes (< 1000 Å) with an ordered atomic structure which are dispersed in a structurally less ordered matrix. The concept of antiphase domains, which are understood as neighboring regions that have the same atomic structure but are shifted relative to each other by a certain fraction of the translation vector, appeared as early as the 1940s [33], and it is usually this structure that is assumed in ordered alloys (see monographs [34, 35]). A modern description of this mechanism can be found in review [36]. A substantiated concept indicating that another type of microstructure is possibly formed in ordering alloys was suggested in the 1970s. This alternative concept assumes that bulk clusters with long-range order emerge in the arrangement of atoms embedded in a disordered matrix and is based on the analysis of diffuse X-ray scattering [37] and the results of transmission electron microscopy [38, 39].

Diffraction effects in the presence of APD or disperse clusters in a crystal structure mainly relate to the width (in the general case, to profiles) of diffraction peaks and differ significantly for these two cases. The differences only consist to a first approximation in the dependence of the peak widths on the Miller indices. In the case of a structure formed as an APD, the width depends on the symmetry of the crystal lattice and on the specific set of Miller indices. For example, only diffraction peaks with odd Miller indices are broadened in the case of the Fe_3Al superstructure [35]. On the contrary, the broadening of the peaks for a structure in the form of a matrix with clusters dispersed in it only depends on the absolute value of the vector in reciprocal space, rather than on its direction in the lattice. The magnitude of the broadening effects is also different for these two cases. The sizes of neighboring domains separated by a coherent antiphase interface are usually comparable; therefore, the width of superstructure peaks in the APD model is increased relative to that of the fundamental peaks by a factor of 2–3. The difference between the broadening of peaks from the matrix and clusters in the model of dispersed clusters can be very large (by a factor of 10 or more).

The hypothesis about the relationship between high magnetostriction values with nanoscale clusters and various variants of short-range order appeared in the literature immediately after the publication of Clark's first papers. The simplest version was based on the assumption that gallium atoms tend to form oriented pairs, i.e., create a quasi-B2 structure in separate, very local areas (see, for example, [40, 41]). Somewhat later, a combination of B2 cells was considered instead of individual cells, leading to the m-$D0_3$ structure (Fig. 5). The idea to combine two oriented pairs of gallium atoms and thereby explain the increase in magnetostriction was apparently presented for the first time in [42]. A more complex structurally inhomogeneous model was proposed in [2], where the tetragonal structure of $D0_{22}$ was considered to be nanoprecipitates. A model that takes into account the role of magnetism in the formation of various types of short-range order was considered in [43] (see also thesis [44]).

Studies [45] (scattering of neutrons by single crystals with various x), [46] (scattering of synchrotron radiation by single crystals with various x), and [47] (X-ray scattering by a single crystal with $x = 18$) are examples of comparatively recent experimental studies of the initial stage of cluster formation in the form of regions with short-range order in Fe–xGa compositions. The short-range order correlation length determined in these studies varies from 6 to 20 Å. An analysis of diffuse scattering along various crystallographic directions enabled an estimation of the shape of the short-range order regions. For example, it was shown in [46] that they are slightly elongated along the [111] direction in Fe–xGa at $x < 18$, while the regions become spherical at $x > 18$.

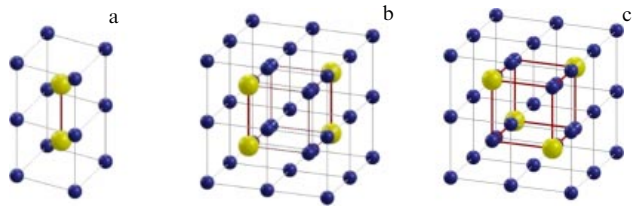

Figure 5. (Color online.) Oriented pairs of gallium atoms (yellow balls), from which two unit cells with the B2 structure (a) and the m-$D0_3$ cell (b) were formed. The $D0_3$ cell (c) is shown for comparison.

Very detailed model calculations carried out in [48] to substantiate the APD model showed that short-range order regions with a characteristic size of $L \approx 20$ Å dispersed in a disordered matrix emerge at the first stage of ordering. They evolve upon prolonged isothermal annealing in such a way that long-range order clusters are formed from them, from which antiphase domains are subsequently created throughout the entire volume of the material. Thus, a microstructure in the APD form should be considered the limiting case of a cluster microstructure.

It should be noted that the concept of structurally ordered clusters in alloys is not strictly defined, as is shown, for example, in monograph [49]. A correct description of the transition from short-range order to long-range order requires an analysis of the atomic distribution functions of higher orders, which in fact has never been done. Computer simulation of the ordering process predicts the emergence of interpenetrating regions with blurred boundaries and complex topology. However, this type of correlated disorder cannot be described as a two-phase system, since there are no spatially defined regions of phases or an interface between them. A complete quantitative analysis requires in this case the use of the transition state cluster model to describe 3D diffuse scattering distributions. A review of work on this topic, which analyzed diffuse scattering in nonstoichiometric compounds, is presented in [50].

As to Fe–xGa and Fe–xAl alloys, the data needed for the analysis of the transition state are still lacking. Therefore, the concept of a cluster will be used in what follows in the diffraction sense, i.e., it will be understood as a connected region, the degree of order in which is higher than in the matrix. A certain characteristic size can be assigned to a set of such regions, which determines an additional (size) contribution to the width of the distribution of diffuse scattering or diffraction peaks. The transition from the distribution width to the characteristic size is carried out in the case of diffraction scattering using the Scherrer or Williamson–Hall approximations [32]. There is apparently no clear boundary between diffuse and diffraction scattering; the width of the superstructure maxima will smoothly decrease with an increase in the cluster size, while their intensity will smoothly increase with an increase in the degree of order in the clusters.

The concept of the morphology of ordered regions can be made more certain by analyzing the profiles of diffraction

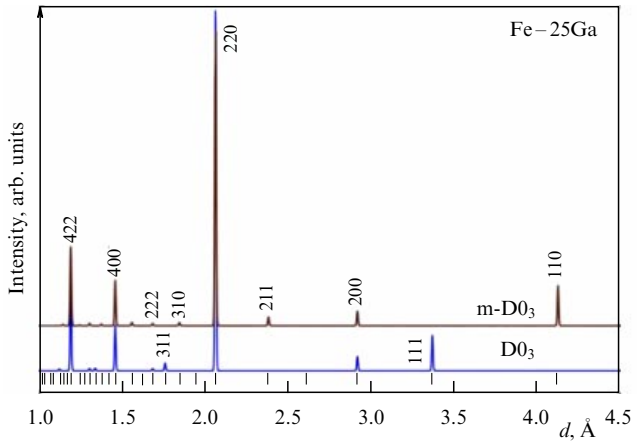

Figure 6. Model powder diffraction patterns for the $D0_3$ and m-$D0_3$ structures calculated for the Fe–25Ga composition with $a = 5.834$ Å. Vertical dashes show the calculated positions of the peaks in a primitive cubic cell without any extinctions.

maxima. For example, if they are described by 3D Lorentz functions, the ordering parameter ξ is distributed in a fluctuation manner, that is, the boundaries of the regions are blurred. If the profiles of the maxima decrease faster, for example, according to a Gaussian profile, it may be asserted that a two-phase structure is formed. The known methods for analyzing the size distribution of coherent scattering regions [32], which are based on mathematical processing of peak profiles, do not appear to be reliable in the case of a cluster state, since the intensity of superstructure peaks is small and, consequently, the profile shape fluctuations are large. There is no doubt from general considerations that there is a distribution of ordered clusters by size, and the width of this distribution can be significant (~ 100 Å or more). Moreover, there should be a distribution by the degree of ordering in addition to the size distribution of clusters. For example, a hierarchical structure with various levels of ordering is conceivable: local inclusions with an order close to perfect state are embedded in areas whose level of ordering is already higher than that of the matrix. Unfortunately, it should be admitted that adequate experimental methods for extracting the corresponding information are lacking as yet.

We now consider the knowledge about the formation of the most frequently considered nonstandard structures in Fe–Al and Fe–Ga: $D0_{22}$, m-$D0_3$, and $L6_0$. The structures $D0_3$ and m-$D0_3$ (see Fig. 5) differ by the positions of Fe and Ga in the inner cube, which becomes the bcc unit cell of the A2 phase upon disordering of the structure. It was hypothesized in [42] that such a rearrangement can lead to tetragonal distortion of the lattice and, as a consequence, to an increase in magnetostriction. In addition, structural factors were calculated in this study, and it was indicated that m-$D0_3$ should yield other superstructure peaks that differ from the normal $D0_3$ structures. Indeed, the model calculation (Fig. 6) shows that there are no superstructure peaks where all indices are odd (for example, 111) in the case of m-$D0_3$, but there are peaks with mixed indices (for example, 110, 211, 310). The intensities of the allowed superstructure peaks are comparable for both structures, while the intensities of the fundamental peaks, i.e., those for which $h + k + l = 4n$ (for example, 220, 400 in the $D0_3$ cell) are the same.

Many experimental studies have been published after Ref. [42], in which, in the opinion of the authors, the formation of regions with the m-$D0_3$ structure was confirmed or refuted. A typical example is Ref. [51], where the presence of m-$D0_3$ was confirmed on the basis of the splitting of diffraction peaks and observations of TEM images for the Fe–15Ga composition. An opposite example is Ref. [52], where eight Fe–xGa single crystals with $8.6 \leqslant x \leqslant 35.2$ were studied (using TEM and SXRD), and m-$D0_3$ was not found in any of them. It was rightly noted in the same study that the splitting of peaks in the XRD spectra observed in [51] may occur for various reasons, in particular, due to surface deformation during sample preparation or precipitation of a phase with a lower gallium content on the sample surface.

Evidence that regions with the m-$D0_3$ structure form under certain conditions was presented in [53, 54]. Fairly clear electron diffraction patterns corresponding to the m-$D0_3$ structure were observed in Ref. [53] for a textured ribbon ~ 50 μm thick with the Fe–17Ga composition obtained by sputtering from a melt. SXRD, SSAS (small-angle synchrotron radiation scattering), and EXAFS (extended fine structure of the X-ray absorption spectrum) spectra were studied in [54] using the Fe–17Ga composition in the form of single crystals with various orientations and a textured ribbon ~ 60 μm thick. A splitting of the diffraction peaks was observed in the diffraction spectra from the ribbon; however, it only occurred for peaks from some of its sections. The relative difference between the parameters of the unit cells of the A2 matrix and the m-$D0_3$ inclusions was $\Delta a/a \approx 0.0028$. Of no less interest is the splitting of peak 103 of the A2 phase noted by the authors of [54]. In their opinion, this is the first experimental observation of the previously predicted tetragonal distortion of the A2 matrix. The degree of distortion is very small, namely $\delta = (c - a)/c \approx 0.0007$, and it can only be noticed if the diffractometer resolution is very high. It was obtained from the SSAS data under the assumption of a Gaussian-type size distribution of nanoprecipitates that they are spherical with $R = (14 \pm 3)$ Å, and their volume proportion is about 1%. This is sufficient in principle to observe the m-$D0_3$ phase in a bulk sample, but the authors of [54] claim that they failed to find any signs of it in the Fe–17Ga single crystal.

We now consider the situation with the $L6_0$ and $D0_{22}$ phases using the example of recent study [55], in which the Fe–26Ga and Fe–27Ga compositions were studied using XRD (bulk polycrystals) and HRTEM (films ~ 80 μm thick). Blurred superstructure spots were found in the HRTEM spectra of the quenched Fe–27Ga sample at the positions of 211 sites of the $D0_3$ phase, which were assigned diffuse scattering by $L6_0$ nanoprecipitates. The size of these formations increased to 100–800 Å after annealing the film for 1 h at 450 °C, and peaks 211 became significantly narrower. The authors note that the bulk density of regions with the $L6_0$ structure also increased, but failed to estimate its value. SAED (Selected Area Electron Diffraction) patterns were obtained for the Fe–26Ga composition, the analysis of which led the authors to the conclusion that they correspond to the $D0_{22}$ structure (they noted that this was the first observation of the $D0_{22}$ structure in Fe–26Ga alloys). A new concept for the formation of the $L1_2$ structure from A2 and $D0_3$ was proposed in [55] based on the experimental data obtained. Namely, it was assumed that structural transitions A2 $\rightarrow$ $L6_0 \rightarrow L1_2$ and $D0_3 \rightarrow D0_{22} \rightarrow L1_2$ are possible (for more details, see Section 6). It was also hypothesized in this study that the observed formation of the $L6_0$ and $D0_{22}$ structures can be considered a basis for explaining the giant magnetostriction in Fe–Ga alloys.

It should be noted in this regard that based on energy considerations there is at present no doubt that the m-$D0_3$ ($L6_0$) and $D0_{22}$ structures can be formed in Fe−Ga compositions. Similar to $D0_3$, they are nonequilibrium, and the difference in the total energy of their formation is small (at the level of 0.2 eV per formula unit). Consequently, similar to $D0_3$, their formation is quite probable in the process of quenching or under certain annealing conditions. As for the diffraction data, there are several points that remain unclear. For example, the volume fraction of regions with m-$D0_3$ ordering detected using TEM is usually sufficiently large to observe not only the fundamental but also superstructure peaks using SXRD or ND. However, no diffractogram (except for electronic) has been published yet where the corresponding superstructure peaks would be present. Moreover, the splitting of the peaks is clearly visible in the diffraction patterns for ribbons prepared in a special way; however, it is absent in the diffraction on bulk samples performed with a resolution sufficient for its observation. The same remark applies to the $D0_{22}$ structure observed in [55]. Moreover, despite the validity of the assertions that tetragonal distortions of the structure introduced by nanoprecipitates should contribute to increased magnetostriction, their small number can hardly affect such a property of bulk nature as magnetostriction.

5. Correlation of the microstructure of Fe−Al and Fe−Ga alloys with their magnetostriction

Attempts have been made in a fairly large number of studies to find some correlation of the functional properties of Fe−Al and Fe−Ga alloys, primarily magnetostriction, with the specific features of their microstructure organization. Of particular interest are naturally those studies in which correlations are analyzed systematically for a wide range of Al and Ga concentrations. We consider the results that were obtained for Fe−Ga using diffraction of synchrotron and neutron radiation.

Polycrystalline Fe−xGa compositions with $14 \leqslant x \leqslant 31$ and a step of 1% (18 samples) were analyzed in [56] using high-energy synchrotron radiation diffraction (HE-SXRD), $E = 105$ keV, which corresponds to $\lambda = 0.1181$ Å. Such a short wavelength enabled a significant increase in the depth of radiation penetration into the samples, each of which was a cylinder 2 mm in diameter. However, on the other hand, Bragg diffraction was observed at very small scattering angles due to the short wavelength. For example, peak 220 for the $D0_3$ phase was located at $2\theta \approx 3.3°$, and, due to the large geometric contribution to the resolution function ($\Delta d/d \sim \Delta\theta/\tan\theta$, where $\Delta\theta$ includes all geometric uncertainties of the scattering process), the peak width was relatively large ($\Delta d/d \approx 0.0030$), and the observation of its tetragonal splitting, as in [54], turned out to be impossible.

In addition to the standard measurement of diffraction spectra, relative changes in the interplanar spacing for fundamental peak 200 were measured in [56] for some of the samples with an external magnetic field of 0.76 T applied. The obtained dependence with two peaks at $x \approx 18$ and $x \approx 27-28$ repeated unexpectedly the behavior of the magnetostriction constant $(3/2)\lambda_{100}$ in Fe−xGa shown in Fig. 1. The surprising feature of the coincidence is as follows. It can be found from the experimental data presented by the authors and simple calculations that the width of peak 200 is approximately $(\Delta d)_{200} \approx 0.0038$ Å, and the displacement of the peaks under the effect of the field, Δd, varies from 0.00006 to 0.00018 Å (depending on the segment of the dependence presented in [56]), i.e., the peak shifted by (1/20−1/60) of its width. Measuring of such small displacements on a set of samples and obtaining at the same time a regular dependence is a very challenging problem.

An analysis of these and other results enabled the authors of [56] to identify four regions with changes in characteristics in the studied range of Ga concentrations. In region I, at $x < 18$, the alloys are in the A2 phase; the cell parameter increases linearly with an increase in the Ga content; and no signs of any ordered regions are observed — there are no superstructure peaks and no broadening or splitting of the fundamental peaks. In region II, up to $x \approx 24.5$, there are superstructure peaks from clusters of the $D0_3$ phase, and the cell parameter changes nonlinearly with a minimum at $x \approx 23.5$. In region III, up to $x \approx 27.5$, where magnetostriction reaches its second maximum, the intensity of superstructure peak 111 attains its maximum and, as suggested by the authors of [56], the entire volume of the sample is occupied in this region by the $D0_3$ phase. At $x > 28$, region IV, the intensity of peak 111 rapidly decreases, while the intensity of peak 200 continuously increases, from which one can conclude that the $D0_3 \rightarrow B2$ transition begins. The authors associate the increase in the width of fundamental peak 200 in region II at $x \approx 21-23$ by a factor of ~ 2 with the emergence of strong strains in the matrix due to the large number of emerged clusters of the $D0_3$ phase.

Most of the results obtained by the HE-SXRD method and published in [56] were confirmed and, in addition, refined and expanded in neutron experiments carried out later [57, 58]. Two sets of Fe−xGa samples with $9.0 \leqslant x \leqslant 32.9$ were studied with the initial state as cast and after air cooling. All the results discussed in this section were obtained using an HRFD TOF diffractometer in the high resolution mode ($\Delta d/d \approx 0.0015$). The evolution of the phase state of the Fe−xGa compositions was traced using three characteristics: the presence of superstructure peaks in the diffraction spectrum (examples of characteristic spectra are given in [57]), the ratio of the widths of the fundamental and superstructure peaks, and the behavior of the intensities of superstructure peaks. Based on these features, the studied range of Ga content was divided into four groups, essentially the same as in [56], but with slightly shifted boundaries of the intervals. They are shown in Fig. 7 along with the behavior of the cell parameters, which were determined from the positions of the fundamental peaks. The behavior of the above characteristics is almost identical within these groups for both types of samples (*as cast* and *air cooled*); namely, it turned out that:

(1) $x < 19$, structure A2, the growth the cell parameter changes at the end of the interval from linear to nonlinear; and the widths of all peaks are described by the same dependence;

(2) $19 \leqslant x < 23$, $D0_3$ clusters are dispersedly distributed in the A2 matrix; the cell parameter decreases; the widths of the fundamental and superstructure peaks are described by different dependences;

(3) $23 \leqslant x \leqslant 27$, homogeneous $D0_3$ structure; the cell parameter increases; the intensity of peak 111 attains its maximum; and the widths of all peaks are described by the same dependence;

(4) $x > 27$, gradual transition $D0_3 \rightarrow B2$.

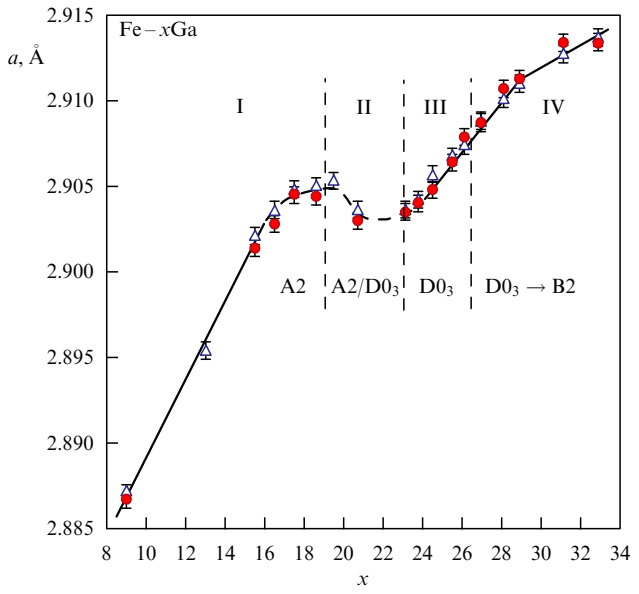

Figure 7. Unit cell parameters of Fe – xGa compositions in the *as cast* (triangles) and *air cooled* (circles) states as a function of the gallium content. The parameters were determined using the positions of the fundamental diffraction peaks. Four types of areas are designated, the description of which is given in the text. For the D0$_3$ phase, the parameter $a' = a/2$ is specified.

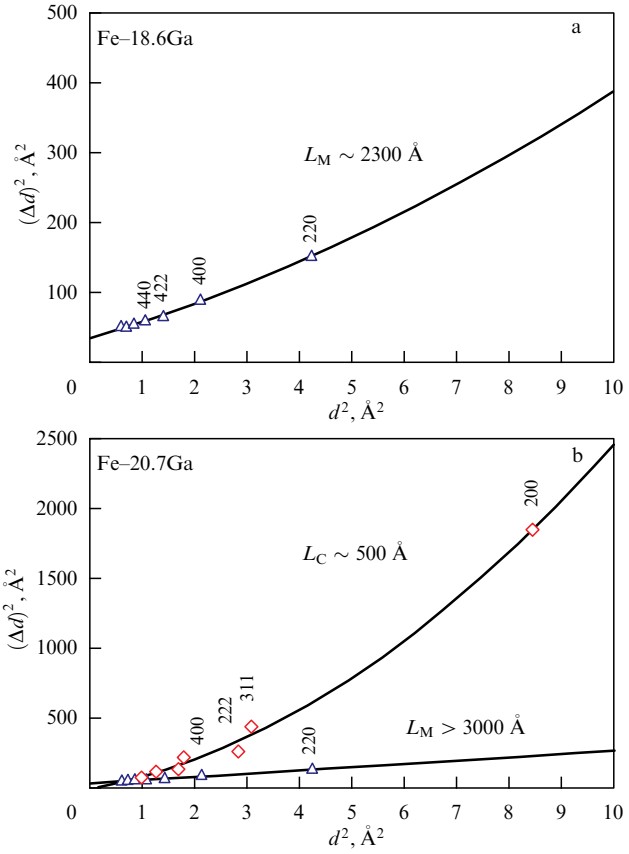

Figure 8. Williamson–Hall plot for the width of the peaks of compositions Fe – 18.6Ga (a) and Fe – 20.7Ga (b). Points corresponding to fundamental peaks are indicated by triangles, to superstructure peaks, by diamonds; L_M is the characteristic CSD size for a disordered matrix, L_C is the characteristic CSD size for ordered clusters. The (Δd) values are multiplied by 10^3.

A somewhat later analysis of the structure of the Fe – 19.5Ga single crystal based on the SXRD data [19] revealed that the intensity distribution in superstructure reflexes, which correspond to D0$_3$ ordering and are broadened in comparison with the fundamental peaks, has a Lorentzian shape. As noted in Section 4, this form of the correlation function does not correspond to any physical object in real space.

A conspicuous feature in the behavior of the cell parameter is the occurrence of a minimum at $x \approx 21-23$. The phenomenon of the decrease in the unit cell parameter in the transition from a disordered to an ordered state was well known long ago for Fe – Ga binary alloys (see, for example, [34, p. 215]); the experimental data displayed in Fig. 7 clearly demonstrate the transition from A2 to D0$_3$, which occurs in the range $17 \leqslant x \leqslant 23$. A similar dependence was obtained in first principle calculations [59]. Of interest is the fact that the deviation of the increase in the cell parameter with increasing Ga content from the linear dependence occurs significantly earlier than the superstructure peaks appear in the diffraction spectra. This implies that the cell parameter turns out to be a characteristic more sensitive to the incipient formation of D0$_3$ phase clusters than the intensities of diffraction peaks. The deviation actually begins at $x \approx 17$, i.e., before the first maximum of magnetostriction; this observation agrees with the information from experiments on diffuse and small-angle scattering that the formation of short-range order begins in this specific region of the Ga content.

Owing to the high resolution of the HRFD, it is possible to obtain reliable data on the behavior of the width of the fundamental and superstructure peaks, which provides important additional information on the microstructural state of alloys. Typical dependences of $(\Delta d)^2$ on d^2 for alloys with various Ga contents are shown in Fig. 8 (see also Fig. 4). It is this kind of result that is fundamental for conclusions about the development of the cluster state of the microstructure of compositions with $19 \leqslant x \leqslant 23$. There are no superstructure peaks in the case of the composition Fe – 18.6Ga (phase A2); the widths of the fundamental peaks lie on a single curve that corresponds to formula (2), wherein the coefficient at d^4 determines the characteristic size of the CSD in the matrix, which is $L_M \approx 2300$ Å. In the case of the composition Fe – 20.7Ga, the diffraction spectrum contains both types of peaks, fundamental and superstructure, and the widths of the diffraction peaks are described by two different dependences. It is almost linear for the fundamental peaks, i.e., CSD sizes exceed 3000 Å, while for superstructure ones it is parabolic, and the coefficient at d^4 of which was used to determine that the characteristic CSD size in clusters is $L_C \approx 500$ Å. The diffraction spectra of compositions with $x \geqslant 23$ contain both fundamental and superstructure peaks (phase D0$_3$), but their widths lie on a single dependence (see Fig. 4), which implies that the microstructure of these compositions is homogeneous. Estimates of the characteristic sizes of clusters obtained using the Williamson–Hall method and the Scherrer formula for peaks 111 and 200 yielded consistent results: their linear growth occurs in the range $20 \leqslant x \leqslant 23$ from ~ 200 to ~ 2000 Å to stabilize at this value.

It should be emphasized once again that the quoted values for L_{coh} of the clusters are the characteristic sizes of coherent scattering regions in them, which can be significantly smaller than the sizes determined by means of optical or electron

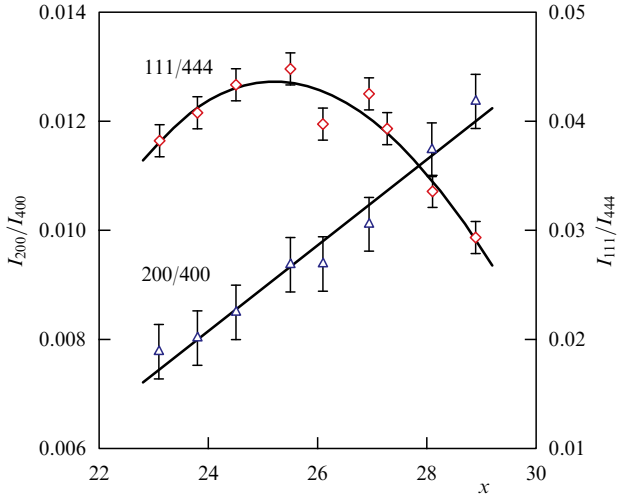

Figure 9. Intensity ratios of reflection orders (superstructure/fundamental) for 111/444 (right scale) and 200/400 (left scale). (Figure taken from Ref. [58].)

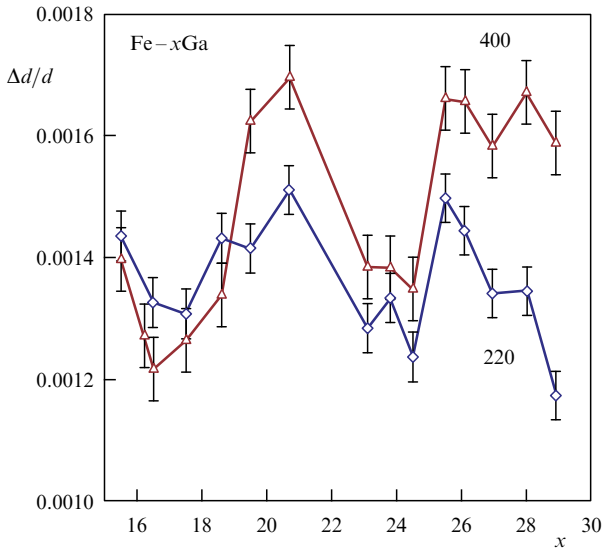

Figure 10. Widths of fundamental peaks 220 and 400 (relative units) as a function of Ga content. The contribution to width from the resolution function is subtracted.

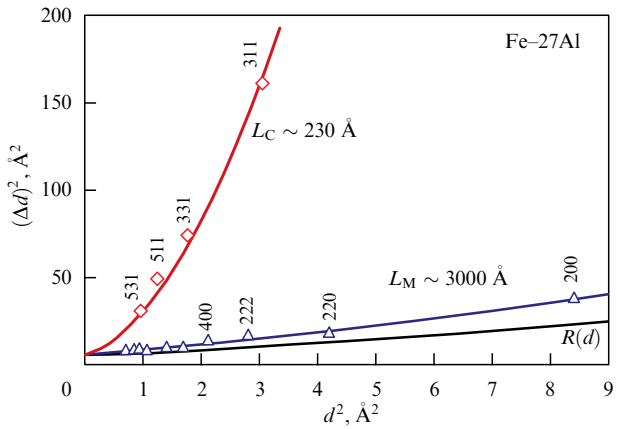

Figure 11. Values of $(\Delta d)^2$ as a function of d^2 for the Fe–27Al alloy. The widths of the fundamental and superstructure peaks allowed in the B2 phase (triangles) fit a dependence close to linear, while the width of the peaks only allowed in the $D0_3$ phase (diamonds) are described by a quadratic dependence. The parameters of the quadratic dependence correspond to the average size of CSD clusters $L_C \sim 230$ Å. The width of the B2 phase peaks is close to the contribution from the HRFD resolution function (lower line). The (Δd) values are multiplied by 10^3. (Figure taken from [60].)

microscopy if the cluster periphery does not have a sharp boundary. If the inevitable distribution in size and degree of ordering is taken into account, it becomes apparent that the numbers for L_{coh} are nothing but estimates that only represent the order of magnitude and the pattern of their changes.

Figure 9 shows that the intensity of superstructure peak 111, which characterizes the $D0_3$ phase, and peak 200, which characterizes the B2 phase, behave in a regular manner. To remove possible texture effects, the intensity ratios of the orders of reflection were calculated; the dependences of the intensity ratios on the Ga content turned out in general to be similar to those obtained by the HE-SXRD method in [56]. A decrease in the intensity of peak 111, which starts from $x \approx 27$, concurrent with a continuing linear increase in the intensity of peak 200, indicates a change in the $D0_3$-type ordering in favor of B2-type ordering. No distinguished regions are formed in this case, since all peaks (both fundamental and superstructure) remain narrow, i.e., the CSD size is large. The dependence of the width of the fundamental peaks on the Ga content was determined (Fig. 10), which turned out to be different from that in Ref. [56] and, on the whole, similar to the x-dependence of magnetostriction with two maxima. Two reasons for this behavior of the peak width can be suggested: an increase in lattice microstresses or a growth of tetragonal distortion of the structure in the ranges $x \approx 19-20$ and $x \approx 26-28$. The first mechanism may be associated with internal strains that emerge in the region where the cluster structure is formed (range 1) and at the beginning of the $D0_3 \rightarrow B2$ process (range 2). The second mechanism may be due to an increase in spontaneous magnetostriction in these ranges and, as a consequence, an increase in tetragonal distortion. To make a selection from the possible options, it is necessary to measure the diffraction spectra with a resolution better than 0.001.

The results for the Fe–xAl compositions published in [60, 61] are similar to the those obtained for Fe–xGa: the same $A2 \rightarrow D0_3 \rightarrow B2$ transitions with increasing x and the same behavior of the cell parameter, but with the minimum shifted to the region $x \approx 35$. It is noteworthy that clusters of the well-ordered $D0_3$ phase in Fe–27Al are not formed in the completely disordered state A2, as in Fe–xGa, but in the B2 structure, which is more ordered than A2 but less ordered than $D0_3$. Proof of this is provided by the Williamson–Hall plot shown in Fig. 11, which shows that the widths of peaks with even Miller indices, allowed in the B2 phase, fall on the linear dependence, while the widths of peaks with odd Miller indices, only allowed in the $D0_3$ phase, lie on the parabolic one. An estimate of the characteristic CSD sizes for the matrix (B2 phase) and clusters ($D0_3$ phase) yields ~ 3000 and ~ 230 Å, respectively.

The presented results (obtained by synchrotron radiation and neutron techniques) provide unambiguous evidence of a clear correlation between the structure (phase state) and microstructure of Fe–Ga and Fe–Al alloys with the behavior of their magnetostriction constant. However, it should be noted once again that the final step — under-

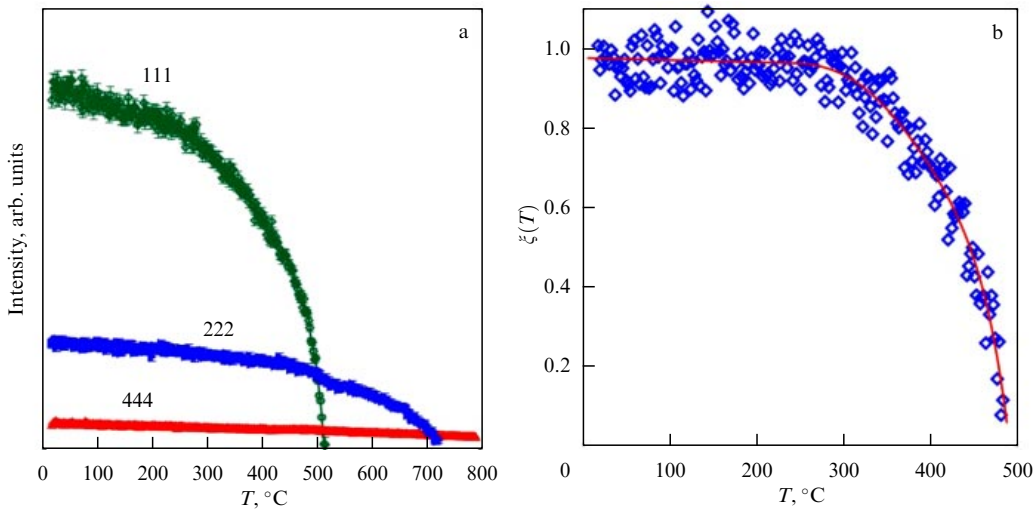

Figure 12. Changes in the intensity of the orders of reflection from the (111) plane of an Fe–27Al single crystal (a) and the parameter that characterizes the degree of ordering of the $D0_3$ structure (b) as a function of the temperature of heating. (Figures taken from [61].)

standing the physical reasons for this correlation — cannot be made as yet.

Of no less importance is obtaining, along with the data on the microstructure of the Fe–Al and Fe–Ga alloys, comprehensive information on the occurrence of structural phase transitions in such compositions and on the processes accompanying them. Neutron diffraction enabled significant progress along the path described, and it is these issues that will be discussed in the next section.

6. First- and second-order phase transitions in Fe–Al and Fe–Ga

Only three structural phases, A2, B2, and $D0_3$, exist in Fe–xAl in the range up to $x \approx 50$, and if the samples are heated or cooled, phase transitions only occur among these phases. A detailed analysis of the dependence of the unit cell parameter on the Al content [62] and the data obtained in [63] for the x-dependences of the cell parameters, peak widths, and their intensities shows that, in the range $0 \leqslant x \leqslant 23$, the main phase is A2, then up to $x \approx 32$, the state is mixed, A2 + $D0_3$ or B2 + $D0_3$, and, depending on the temperature regimes, the $D0_3$ phase can be present in the form of clusters with sizes of several hundred angstroms or occupy the entire volume of the sample. Studies [60, 61, 63] report data on phase transitions upon slow heating and the subsequent cooling of compositions with $x \approx 27$, 31, and 50 and upon replacing part of Al with Cr [64]. The most complete results including data for a single crystal (Fig. 12) were obtained for Fe–27Al. The intensity of peak 111, which is only allowed in the ordered $D0_3$ phase, decreases to zero at $T \approx 500\,^{\circ}\mathrm{C}$, then, at $T \approx 720\,^{\circ}\mathrm{C}$, peak 200, which characterizes the less ordered B2 phase, disappears, and the sample structure becomes disordered. A joint analysis of the temperature dependences of the intensity and width of peak 111 made it possible to establish the behavior of the order parameter in the $D0_3$ phase. The new data obtained have reliably confirmed that the structural transformations $D0_3 \rightarrow B2 \rightarrow A2$ observed in Fe–xAl up to $x = 31$ are typical second-order transitions.

If the Fe–27Al composition, after being maintained at 900 °C, is quenched in water, its state corresponds to the B2 structure. If heating is slow (2 °C min^{-1}), B2 → $D0_3$ →

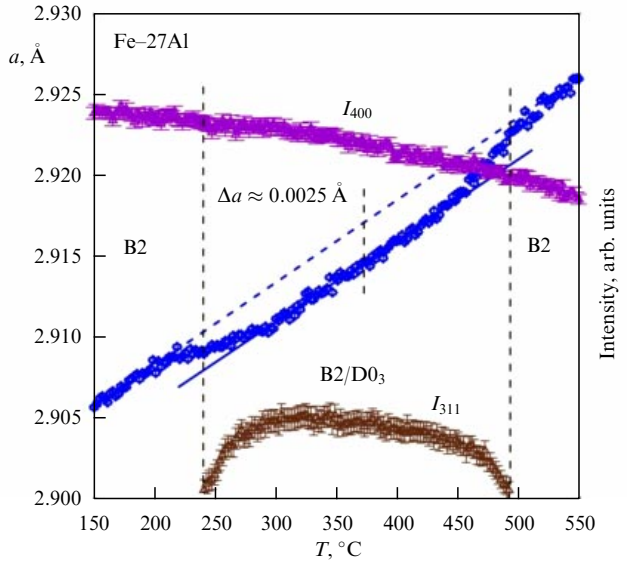

Figure 13. Temperature dependences of the matrix unit cell parameter (left scale) and intensities (right scale) of the fundamental (I_{400}) and superstructure (I_{311}) peaks of the $D0_3$ phase measured in heating an Fe–27Al composition. When clusters of the ordered $D0_3$ phase appear and disappear, the cell parameter in the B2 matrix deviates from the linear temperature dependence. Miller indices of diffraction peaks are given for a $D0_3$ phase cell. (Figure taken from [63].)

B2 → A2 transitions occur, which are clearly observed in an *in situ* neutron diffraction experiment. The first and second transitions are accompanied by characteristic changes in the linear increase in the cell parameter with temperature. This is shown in Fig. 13, where the behavior of the intensities of the main and superstructure diffraction peaks of the $D0_3$ phase is shown along with the cell parameter. The microstructure of the sample in the temperature range $240 < T < 490\,^{\circ}\mathrm{C}$ is a matrix of the partially ordered B2 phase with clusters of the ordered $D0_3$ phase distributed in it in a dispersed way. It can be seen that the deviation of the cell parameter from the linear dependence begins slightly earlier than the emergence of superstructure peak 311. It should be noted that the appearance and disappearance of ordering does not affect in

any way the intensity of fundamental peak 400, the slow decrease in which corresponds to the behavior of the Debye–Waller factor.

The development of structural phase transitions in Fe–xGa was studied in a series of our neutron diffraction *in situ* experiments [18, 20, 57, 65–67]. The spectra were basically measured in the mode of heating the sample at a constant rate of 2 °C min^{-1} to ~ 900 °C and subsequent cooling to room temperature. Experiments with several compositions were also carried out at various heating rates (from 1 to 20 °C min^{-1}) and under rapid heating to a certain temperature followed by maintenance at this temperature for several hours. The results obtained are too voluminous to be discussed in detail in this review, and their general idea alone is presented below.

No other structural phases, except for A2, appear in an explicit way in compositions with $x < 19$ in the process of heating-cooling. Compositions with x close to 19 are in a boundary state; in some cases, $D0_3$ phase clusters are observable in them immediately after casting, while in other cases they only appear after heating and cooling. Up to $x \approx 23$, the initial cluster state A2 + $D0_3$ transforms upon heating into A2 + B2, and next into A2. Reverse transitions occur during cooling: A2 → B2 → A2 + $D0_3$. If the gallium content is $x = 27–28$, the overall scheme of transitions becomes more complicated: observed upon heating are the transitions $D0_3 \rightarrow L1_2 \rightarrow D0_{19} \rightarrow$ A2 (see Fig. 3), and upon cooling, A2 → B2 → $L1_2 + D0_{19}$. Some variations of these schemes consist, for example, in the fact that, at smaller x ($x \approx 24$), phases Al and A3 are formed instead of $L1_2$ and $D0_{19}$, and at larger x ($x \approx 29$), the $D0_{19}$ phase is not formed during cooling. It should be noted that small changes in the gallium content may result in significant changes in the sequence of transitions and in the volume fraction of certain phases. For example, the phase transitions in the compositions Fe–25.5Ga and Fe–26.9Ga proceed upon heating in the same way. However, when the Fe–25.5Ga composition is cooled, the $D0_3$ and A3 phases appear and then disappear, and the $L1_2$ phase alone is formed in the final state, whereas in Fe–26.9Ga, the $L1_2$ and $D0_{19}$ phases are represented in the final state in almost equal proportions [68].

A quantitative analysis of the data obtained in *in situ* experiments consists in determining the intensities, positions, and widths of a number of fundamental and superstructure diffraction peaks. The intensities of the fundamental peaks are used to establish the temperature dependences of the volume proportions of the structural phases, and their positions, to determine the unit cell parameters and the atomic volume (cell volume per atom) (Fig. 14). The behavior of the volume fractions of the phases may be used to determine the rate at which the transitions take place and in what temperature range they occur, while the behavior of the atomic volume shows, for example, that the transitions $D0_3 \rightarrow L1_2$ and $D0_{19} \rightarrow$ A2 are accompanied by a large jump in the volume, i.e., these are first-order transitions. Analysis of the width of the diffraction peaks makes it possible to estimate the magnitude of the microstresses that arise during the transitions and the degree of their anisotropy. The peak intensities may be analyzed in cases where the texture effects are small using the Rietveld method, as was done in [18], which enables extraction of information on the magnitude of the ordered magnetic moment and the occupancy factors of individual crystallographic positions. Interesting additional information is provided by a comparison of the data obtained

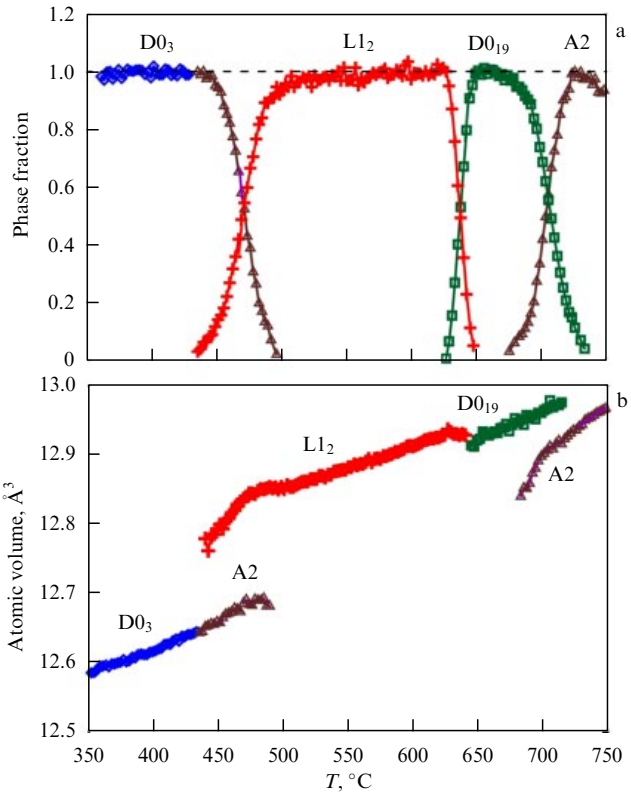

Figure 14. (Color online.) Temperature dependences of the volume fraction of the structural phases (a) and the atomic volume (b) for the Fe–27Ga composition during its heating. (Figures taken from [18].)

during heating at various rates and in several successive heating-cooling cycles. For example, Fig. 15 displays a comparison of the volume fractions of the phases that emerge upon cooling of the Fe–27Ga composition at various rates (1, 4, and 8 °C min^{-1}). It can be seen that, as the cooling rate increases, the temperature at which the $D0_{19}$ and $L1_2$ phases emerge shifts, and at low temperatures the ratio of the phase fractions significantly changes in favor of $L1_2$.

Results of fundamental importance were obtained in *in situ* experiments carried out in the mode of rapid heating to a certain temperature followed by maintaining this temperature for several hours [67]. These experiments made it possible to reveal previously unknown structural features of the first-order transition between differently ordered phases and obtain new data on its kinetics. These results are based on data partially presented in Fig. 16. The samples are initially in the $D0_3$ phase, and when held at a constant temperature, the $D0_3 \rightarrow L1_2$ transition occurs. The figure shows how the temperature changed (heating at a rate of 20 °C min^{-1} and holding at $T = 405$ and 435 °C) and how the intensities of the fundamental and superstructure diffraction peaks associated with the $D0_3$ and $L1_2$ phases changed over time. A specific feature of these dependences is a gap in time between the disappearance of the superstructure peaks of the initial phase ($D0_3$, 111) and the appearance of superstructure peaks of the new phase ($L1_2$, 100). Moreover, there is a small but noticeable gap in time between the disappearance of the peak ($D0_3$, 111) and the appearance of the peak (A1, 200). An unambiguous interpretation of these facts is that, at first, ~ 20 min after the start of heating, i.e., upon reaching $T \approx 400$ °C, the ordered $D0_3$ structure transformed into the disordered bcc state A2. Then, after some time lapsed (this

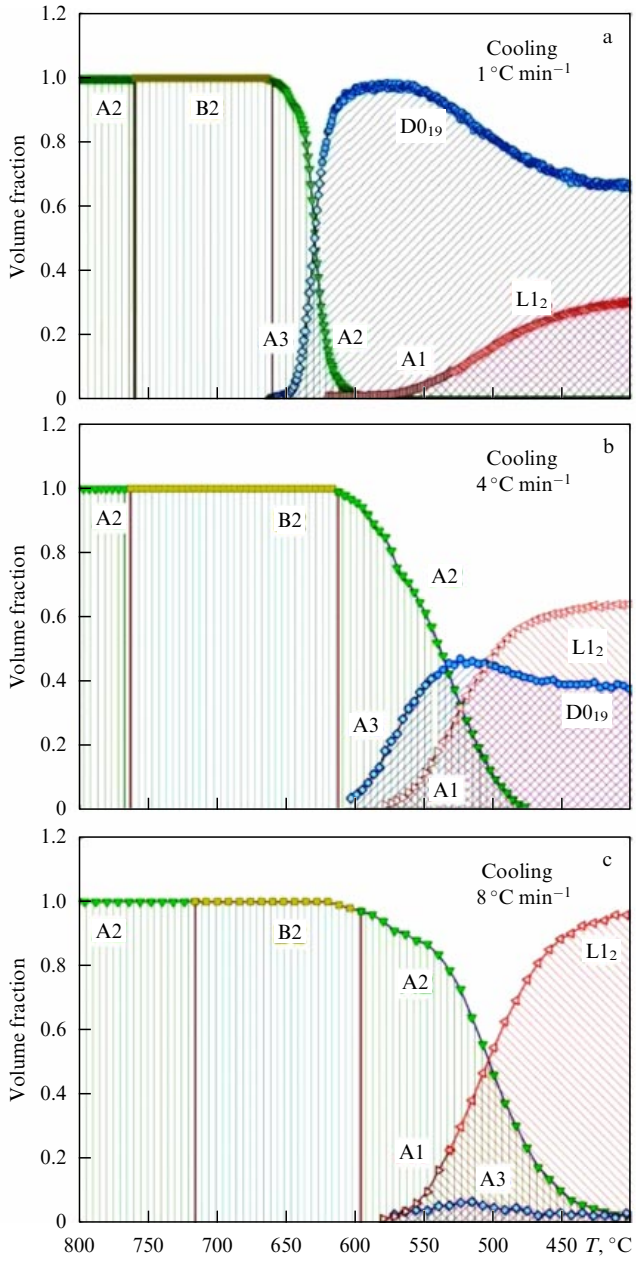

Figure 15. Temperature dependences of the volume fraction of structural phases in cooling the Fe–27Ga composition at rates (a) 1, (b) 4, and (c) 8 °C min^{-1}. (Figure taken from [20].)

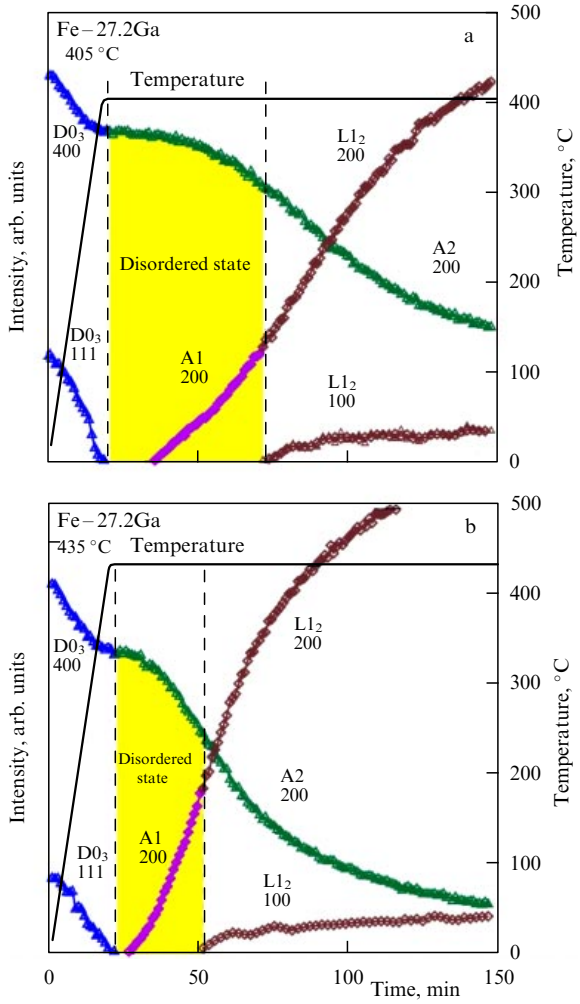

Figure 16. (Color online.) Time variations in the intensities of the fundamental ($D0_3$/A2, 400/200, and A1/$L1_2$, 200/200) and superstructure ($D0_3$, 111 and $L1_2$, 100) diffraction peaks during rapid heating of the Fe–27.2Ga composition and subsequent isothermal holding at temperatures (a) 405 and (b) 435 °C (right scale). The vertical lines indicate the time intervals in which the structure is in a disordered state. The beginning of the time scale corresponds to the start of the rise in temperature. (Figures taken from [67].)

interval diminishes with an increase in the holding temperature), signs of the formation of the fcc structure A1 appear. Finally, the last stage of the process begins after one more incubation period, which consists of the formation of the ordered $L1_2$ structure. On the whole, this process can be represented as a chain of $D0_3 \rightarrow A2 \rightarrow A1 \rightarrow L1_2$ transitions, where the initial and final steps are the second order transitions, and the central transition is the first order one. A specific calculation based on the data on the change in the unit cell parameters of these phases shows that lattice strains in disordering ($D0_3 \rightarrow A2$) and ordering ($A1 \rightarrow L1_2$) are small ($\varepsilon \leqslant 0.001$) and uniform. On the contrary, the $A2 \rightarrow A1$ transition is accompanied by large and inhomogeneous deformations: tension along the fourth-order axis ($\varepsilon_c \approx 0.266$) and compression in the perpendicular plane ($\varepsilon_{ab} \approx -0.105$). It is remarkable that these values differ only slightly from the deformations observed during the α-Fe → γ-Fe transition [31].

The following features of the $D0_3 \rightarrow L1_2$ transition may be distinguished. The atomic volume of the A1/$L1_2$ phases is greater than that of the $D0_3$/A2 phases, although the latter are a bcc structure, which in the case of base metals is less densely packed than fcc. Calculations using the density functional theory [59] confirm this effect, indicating its association with the specific features of the electron density distribution in such alloys. The intensity of the superstructure peak ($D0_3$, 111) decreases faster than that of the fundamental peak ($D0_3$, 400) at the initial segment of the rise in temperature. This implies that the degree of ordering of atoms, i.e., the factor $\xi(T)$ in Eqn (1), begins to decrease even upon slight heating. The time during which a disordered state exists in Fe–27.2Ga, which is defined as the time between the disappearance of the ($D0_3$, 111) peak and the appearance of the ($L1_2$, 100) peak, decreases with increasing temperature as a linear function of $1/T$.

It is of importance to note that doubts may arise regarding the formation of a completely disordered state, since super-

structure peaks are of low intensity, and it can be assumed that they are simply not visible at certain time intervals. However, as can be seen from Fig. 16, the intensity of fundamental peak 400 during the $D0_3 \rightarrow A2$ transition only decreases by $\sim 15\%$; consequently, should the bulk density or ordering factor decrease by the same amount, superstructure peak 111 should be reliably detected. A similar argument can be applied to the fundamental and superstructure peaks of the $L1_2$ phase. By the time peak 100 appears, the intensity of peak 200 is about 20–30% of the maximum, and should superstructure peak 100 have appeared earlier, it would have been detected. Since no diffraction peaks from any other phases were observed during the entire time of the experiment, it can be argued that in the time intervals indicated in Fig. 16 the atomic structure of the studied samples is in a disordered state, first as the A2 phase and next as A2 + A1.

Various versions of how the conversion of $D0_3$ to $L1_2$ occurs can be found in the literature. It was assumed by Khachaturyan and Viehland [2] that this transition can occur through the intermediate ordered tetragonal structure $D0_{22}$. The scheme $D0_3 \rightarrow A1 \rightarrow L1_2$ was considered in [69] on the basis of XRD and TEM data. Study [55] was already mentioned above, in which the $D0_3 \rightarrow A2 \rightarrow L6_0 \rightarrow L1_2$ version was proposed as the main one, and the $D0_3 \rightarrow D0_{22} \rightarrow L1_2$ version, as an alternative. However, all these assumptions were made based on the observation of the initial ($D0_3$), final ($L1_2$), and one or more (as in [69]) intermediate states. The only experiments in which this transition was traced with virtually continuous scanning in time are still the neutron diffraction experiments discussed in [22] and [67].

There are two more important points worth noting. First, the formation of a completely disordered state during a transition between two ordered states is not surprising, since the $D0_3 \rightarrow L1_2$ transition is accompanied by a large jump in the atomic volume ($\sim 1\%$). Second, the transition between the disordered states $A2 \rightarrow A1$ seems to be completely analogous to the α-Fe $\rightarrow$ γ-Fe transition in pure iron, in which the tetragonal distortion of the lattice hypothesized in the Bain model is not manifested in diffraction experiments similar to the Fe–Ga alloy.

7. Relationship of ordering with the crystal lattice

It was already mentioned in Section 5 that the unit cell parameter decreases during the transition of certain types of binary alloys from a disordered to an ordered state. It is illustrated by the data shown for Fe–xGa in Fig. 7. The dependence of the unit cell parameter of Fe–xAl compositions on the aluminum content has the same character [62]; only the minimum is slightly shifted towards higher x ($x \approx 35$ instead of $x \approx 22$ for Fe–xGa).

The reasons for this phenomenon are still a matter of discussion. For example, it is discussed in review [70], based on experimental data for a large number of binary alloys, whether it is related to energy or geometric (difference among ionic radii) factors. The author of Ref. [70] argues that the correlation of the behavior of the parameter with the ordering energy is more pronounced than the correlation with the differences among the sizes of atoms. Hence, it may be concluded that first principle calculations can yield a realistic dependence of the unit cell parameter on the composition, and this was actually confirmed in [59] for Fe–xGa.

An amazing fact which earlier had escaped researchers' attention is that the cell parameters displayed in Fig. 7 for Fe–xGa and presented in [62, 63] for Fe–xAl are determined from the position of the fundamental peaks, i.e., for the matrix, while ordering occurs in the clusters that only occupy a certain (sometimes very small) fraction of the sample volume. A nonlinear change in the cell parameter of the matrix with an increase in the Ga or Al content implies that the matrix is sensitive to the ordering process, first via the short-range and next long-range order, and a very high degree of coherence is maintained between the crystal lattices of the matrix and clusters. Otherwise, one would expect that the matrix cell parameter should increase linearly in a certain range of Ga or Al content (as in the A2 phase). The difference between the cell parameters of the A2 and $D0_3$ phases (reduced to A2) predicted by first principle calculations for Fe–xGa is $\Delta a \approx 0.02$ Å ($\Delta a/a \approx 0.007$). If there were no coherence between the lattices, the profiles of the fundamental diffraction peaks in high-resolution spectra should be a sum of narrow peaks from the matrix and broadened peaks from clusters with a reduced cell parameter. For example, an incoherent mixture of A2 and $D0_3$ should lead to the splitting of peak 400 into two components with $\Delta d \approx 0.01$ Å, which is not observed in neutron diffraction spectra. A specially performed analysis showed that the profiles of the fundamental peaks from Fe–xGa actually reproduce the profiles of the peaks from standard polycrystals used to determine the diffractometer resolution function; i.e., microstresses, the size effect, and the assumed difference between the parameters of the matrix and cluster cells do not introduce any significant broadening or shift.

Moreover, unit cell parameters of these phases can be independently determined for ordered compositions Fe–Al and Fe–Ga that contain phases A2 (as a matrix) and $D0_3$ (in the form of clusters). To do so, the profiles of individual fundamental and superstructure diffraction peaks were analyzed and their positions on the d_{hkl} scale were established, after which the cell parameter value was calculated individually for each peak. Examples of such an analysis (first performed in [60]) are displayed in Fig. 17 for Fe–25Al–9Cr and Fe–23.8Ga. It can be seen that the average values of the cell parameter found in this way are within the range of ± 0.0002 Å, i.e., $\Delta a/a \approx 3.5 \times 10^{-5}$, and this value is tens of times less than the expected differences. It can even be argued that the degree of coherence between the crystal lattices of the matrix and ordered regions is close to 100%.

These neutron diffraction results disagree with the X-ray and synchrotron-diffraction data reported in many studies where the splitting of the fundamental diffraction peaks into two components was observed. The relative difference in the observed positions of the components is quite large and varies within the range $\Delta a/a \approx (1-4) \times 10^{-3}$. This value is ~ 100 times greater than the above estimate of the degree of correspondence between the lattices of the matrix and clusters.

It is noteworthy that the two observed components are interpreted in different studies in the opposite way. For example, obtained in one of the first studies on this topic [71] for peak 422 of the composition Fe–19.5Ga were the values for two observed components $d_1 = 1.1878$ Å and $d_2 = 1.1853$ Å, which correspond to $\Delta a/a \approx 2 \times 10^{-3}$, and the component with d_1 was assigned to the A2 phase. The same interpretation of the splitting of the fundamental peaks in the Fe–29Ga composition is suggested in [72]. Close values of the splitting of the fundamental peaks were found in [53, 54, 73], but the components with a smaller interplanar spacing were assigned to the A2 phase.

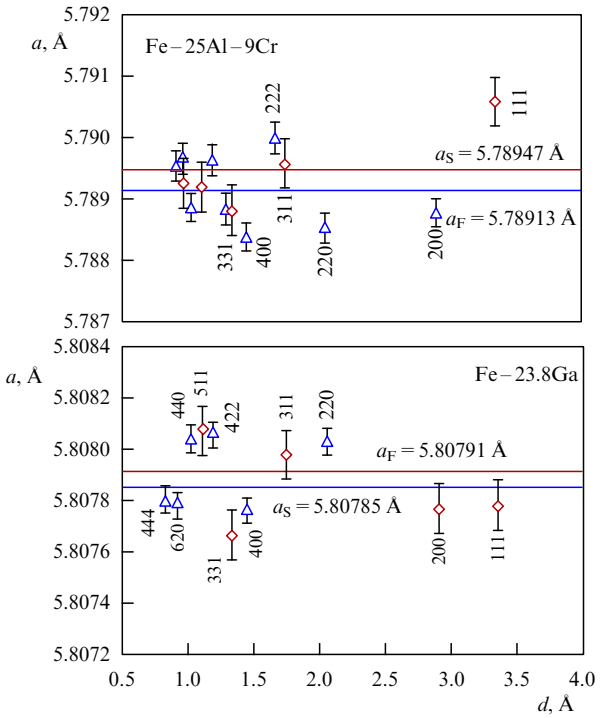

Figure 17. (Color online.) Parameters of unit cells of the matrix (triangles, a_F) and $D0_3$ clusters (diamonds, a_S) for compositions Fe – 25Al – 9Cr and Fe – 23.8Ga determined from the positions of individual (fundamental and superstructure) diffraction peaks. For the composition with Al/Cr, the matrix is the B2 phase, while for the composition with Ga, the A2 phase.

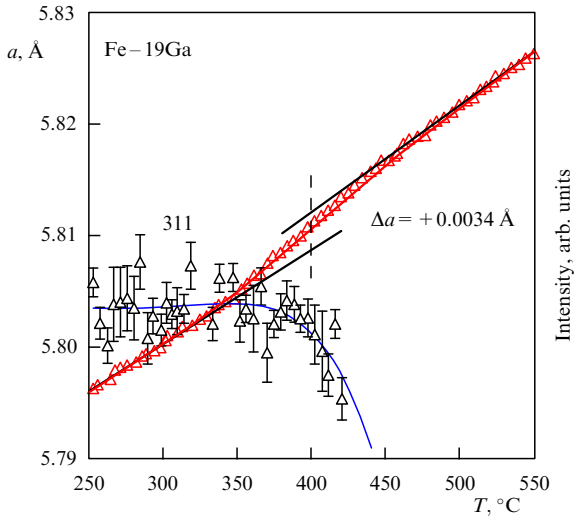

Figure 18. Temperature dependence of the unit cell parameter (left scale) and the intensity of superstructure peak 311 (right scale) of the Fe – 19Ga composition during its heating at a rate of 2 °C min^{-1} in the region of the $D0_3 \rightarrow A2$ structural transition in the matrix. The straight lines connecting the points for the cell parameters are the result of fitting the experimental points by a linear function in the temperature intervals before and after the phase transition. The change in the parameter during transition is indicated.

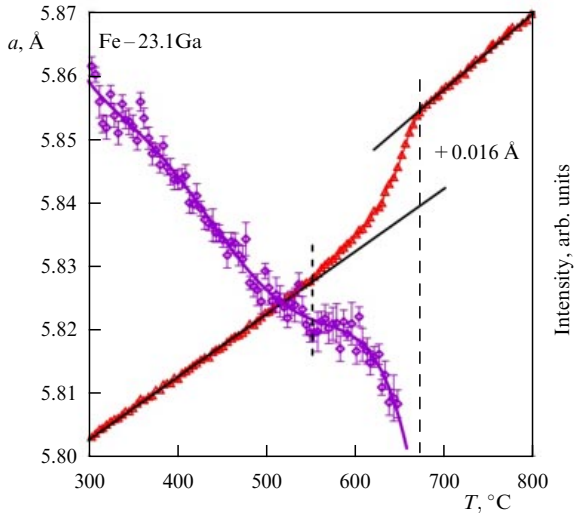

Figure 19. Same as in Fig. 18 but for the Fe – 23.1Ga composition.

These results are inconsistent with the observation that any splitting whatsoever of the fundamental peaks of the A2 and $D0_3$ phases is absent, not only in neutron, but also in X-ray and synchrotron diffraction spectra measured in bulk samples of both Fe – Al and Fe – Ga [56, 58, 62, 63]. The exact reason for these differences is not yet known. One of the possibilities is violation of the coherence of the lattices of the matrix and clusters in thin layers of the material (in films and near the surface), while coherence exists in the bulk. Another reason may be the heterogeneity of the composition, which is more pronounced in thin layers than in the bulk. Some indications of the inhomogeneity of the composition were obtained in [74], wherein it was found that, if the sample is maintained in a vacuum, and this is usually done to prevent its oxidation, the loss of gallium and the formation of a Ga-deficient phase whose cell parameter differs from that of the main phase may occur. Similar results have been obtained recently in studying the effects of heating–cooling of the Fe – 45Ga phase [17].

The effects associated with the coherence of the crystal lattices of the A2, B2, and $D0_3$ phases can also be analyzed using experimental data obtained during phase transitions upon heating or cooling. A typical example of how the cell parameter changes upon ordering and subsequent disordering during the $B2 \rightarrow D0_3 \rightarrow B2$ transitions in Fe – 27Al is displayed in Fig. 13, which shows that the measured jump of the cell parameter is about 0.0025 Å. This value is somewhat less than would be expected based on the data of Ref. [62]. However, the magnitude of the jump should depend on the degree of the attained order and decrease if the order in the clusters is not complete.

The jump in the parameter in Fe – Ga compositions can attain the same or even somewhat larger values. Figures 18 and 19 show combined temperature dependences of the cell parameter of the A2 and $D0_3$ phases and the intensity of superstructure peak 311 during the $D0_3 \rightarrow A2$ transition in the compositions Fe – 19.0Ga and Fe – 23.1Ga upon heating. The deviations of $a(T)$ from the linear dependence upon disordering during heating clearly correlate with the behavior of the intensity. It can be seen, in particular, that these deviations begin significantly earlier than the intensity of peak 311 begins to rapidly decrease, and end later than this peak ceases to be visible. The magnitude of the jump in the parameter clearly correlates with the degree of ordering in the clusters and, apparently, with their bulk density. Thus, its value in the composition of Fe – 23.1Ga approaches the calculated one, which is an indication of an almost complete structural order in the initial state.

Since the unit cell parameter is measured with much better accuracy than the intensity of weak superstructure peaks, it is this specific parameter that can be used to determine the

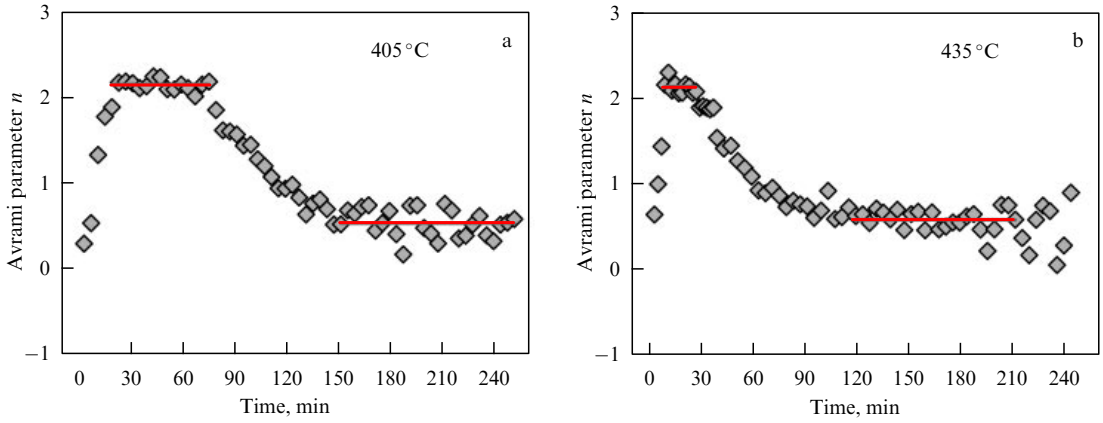

Figure 20. Local Avrami parameter n for the Fe–27.2Ga alloy at (a) 405 °C and (b) 435 °C calculated as a function of time. The red lines show two time intervals where $n(t) \approx$ const. (Figure taken from [67].)

temperature range of the transition. It should be noted that the profiles of the fundamental peaks remain virtually unchanged during these transitions, which confirms the high degree of coherence of the lattices of the matrix and the clusters.

8. Kinetics of phase transitions

Several structural phase transitions occur in heating cast Fe–xGa samples with a gallium content $x \approx 24-29$, of which the first and, perhaps, the most important from a practical point of view is $D0_3 \rightarrow L1_2$. This transition, which is driven by the diffusion mechanism, requires the structure to be rearranged, and its kinetics is slowed down due to the relatively high energy barriers among the positions of atoms in the $D0_3$ and $L1_2$ phases. This transition is used below as an example to outline the type of kinetic data that can be obtained in a neutron diffraction experiment (for more details, see Ref. [67]). A modern presentation of the application of diffraction on polycrystals to the analysis of the kinetics of phase transformations can be found in monograph [75]. It also contains a description of the Johnson–Mehl–Avrami–Kolmogorov approach (JMAK model), which was used in Ref. [67] to process and interpret neutron data.

The JMAK model [76–78] is based on the assumption that several conditions are fulfilled, the account of which enables obtainment of the volume fraction of the formed phase, $f(t)$, as a function of time t after the temperature is set (usually referred to as the Avrami equation):

$$f(t) = 1 - \exp\left[-(kt)^n\right], \tag{3}$$

where k is a kinetic coefficient that depends on temperature, and the exponent n (Avrami parameter), which is determined by the growth conditions and the rate of formation of new phase nuclei, can be fractional. A summary table of the values of n for various combinations of the rate, type, and geometry of nucleus growth can be found in [79].

Equation (3) can be transformed as follows:

$$\ln\left[-\ln(1-f)\right] = n\ln k + n\ln t, \tag{4}$$

whence it is seen that the parameters n and k can be determined from a linear approximation of the experimental dependence of $\ln\left[-\ln(1-f)\right]$ on $\ln t$. Based on the conditions of the classical Avrami model, parameter n, i.e. the slope of the straight line, must remain unchanged during the entire transition; examples of such processes are given in [75].

Cast samples of Fe–27.2Ga and Fe–28.0Ga were heated in HRFD experiments to a specified temperature at a rate of 20 °C min^{-1}, and the diffraction spectra were measured at a specific temperature for $\sim$ 4 h. Isothermal measurements for both compositions were made at nominal temperatures of 405, 435, and 470 °C, which was maintained with an accuracy of $\pm$2 °C. These values were attained in 19, 21, and 23 min, respectively, after the start of the temperature rise. The time required for 50% of the $L1_2$ phase to form ranged — depending on the holding temperature — from 20 to 120 min; therefore, the diffraction spectra were measured every minute, which made it possible to trace the details of the transition.

The time dependences of the integral intensities of the fundamental peaks for $D0_3/A2$ and $A1/L1_2$ were found at the first stage of processing the experimental data, from which the values $f_1(t)$ and $f_2(t)$, the fraction of phases, as a function of time were determined. It was checked that the sum of the volumes occupied by these phases coincides with the volume of the sample with an accuracy of several percent, i.e., the nucleation of the $A1/L1_2$ phases occurs from the volume of the $D0_3/A2$ phases. Further, the dependences $\ln\left[-\ln(1-f)\right]$ on $\ln t$ were plotted for both compositions at all three temperatures of isothermal holding; it turned out that the dependences were not linear throughout the entire process. Differentiation of the obtained dependences made it possible to determine the value of the so-called 'local' Avrami parameter, $n(t)$. The constancy of $n(t)$ is only maintained in the process at relatively small time intervals and, although two intervals may be conventionally distinguished within which $n(t) \approx$ const, this approximation is very rough, since the transition interval is fairly long (Fig. 20).

The values of the Avrami parameter for Fe–27.2Ga at the initial stages of growth of the $L1_2$ phase at all three temperatures of isothermal holding are very close to each other and fall within the range of 1.5–2.5, which, according to [79], is typical of diffusion-controlled growth of new phase grains with a decreasing nucleation rate. The subsequent change in the fraction of the $L1_2$ phase is characterized by a gradual decrease in parameter n to a value of 1.5 or below, which correspond to the situation where the nucleation sites

are exhausted, and the fraction of the new phase increases due to the growth of already existing nuclei. Since $n(t)$, having attained at the last stage of the transition a value of 1.5, continues to decrease to ~ 0.5 at 405 and 435 °C and virtually to 0 at 470 °C, it is inferred that the growth rate of grains of the new phase gradually decreases.

If the temperature increases from 405 to 470 °C, a several-fold decrease in the time of formation of 50% of the $L1_2$ phase occurs (fourfold decrease for Fe–27.2Ga). If the Ga content in the alloy increases to $x = 28$, i.e., the deviation from the stoichiometric composition of Fe_3Ga increases, the rate of transformation of the $D0_3/A2$ phases into $A1/L1_2$ decreases in comparison with Fe–27.2Ga at the same temperatures. For example, the time of formation of 50% of the $L1_2$ phase at a holding temperature of 405 °C is 1.6 times longer for Fe–28.0Ga.

It follows from the results obtained that the kinetics of the entire transition cannot be described within the JMAK model, since the value of the Avrami parameter n does not remain constant with the exposure time, but decreases by a factor of 3–4. This indicates deviations from the conditions for the validity of the model, for example, the nucleation mechanism and the process of the growth of nuclei can change, and collisions of growing grains of a new phase can occur. Nevertheless, it is possible to single out for the local Avrami parameter the sections with $n(t) \approx$ const for which an interpretation may be provided. For example, the Avrami parameter for the initial stage of the transition in the Fe–27.2Ga composition has values close to $n = 2$ for all three temperatures of isothermal holding, which corresponds to the model with a constant growth rate of grains of a new phase with a decreasing nucleation rate. The values of n are significantly lower for the Fe–28.0Ga composition, which may indicate the presence of hidden nuclei of the $L1_2$ phase in the sample.

9. Conclusions

Diffraction of short-wave radiation — electron, X-ray, synchrotron, and neutron — makes it possible to obtain very rich information on the features of the structural arrangement of binary iron-based alloys. The experimental material collected to date seems, at least at first glance, to already be quite sufficient to attempt to draw on its basis some definite conclusions about the physical mechanisms of giant magnetostriction in Fe–Ga alloys. However, despite considerable efforts, this has not been done in a reliable way. The concepts suggested in the literature so far only outline seemingly promising paths to attain this goal. For example, it is universally agreed that, to understand the mechanisms for the formation of enhanced magnetostriction, a deeper understanding of the reasons for the appearance of inhomogeneous structural and microstructural states of these alloys is needed.

The results of neutron diffraction studies are an essential part of the collected experimental material. The bulk-related nature of the information obtained using neutrons made it possible to significantly clarify the situation with various phase states of alloys, structural transitions between them, and the arrangement of their microstructure. It is neutron diffraction that has turned out to be the most informative method for studying phase transformations *in situ* and in real time. The dispersed cluster model, which has been convincingly confirmed in neutron experiments, seems to be the most adequate approach to analyze correlations between the functional properties and the microstructure of alloys. A side, but important, implication of its validity is the need for a new look at the known phase diagrams of Fe–xMe alloys, for which regions of coexistence of ordered and disordered phases have been found, since in many cases the volume occupied by an ordered phase in crystallites does not exceed 50%.

The Fe–Ga alloys have been explored using neutron scattering techniques other than diffraction. For example, small-angle neutron scattering (SANS) was used in [80] to measure spectra for the Fe–19Ga single crystal. It was found that the magnetizations of the clusters with an ordered structure and that of the disordered matrix are different; this difference essentially results in the emergence of magnetic contrast and, as consequence, of small-angle neutron scattering. Based on the similar behavior of the SANS intensity and the magnetostriction constant as a function of the applied magnetic field, the authors reached a conclusion that it is clusters that make a significant contribution to the bulk magnetostriction of the sample.

The effects observed in inelastic neutron scattering were analyzed in single crystals of $Fe_{1-x}Ga_x$ ($x = 10.8$, 13.3, 16.0, and 22.5) in Ref. [81]. The $D0_3$ phase was absent in the compositions with $x \leqslant 16$; however, it occupied $\sim 24\%$ of the volume in the sample with $x = 22.5$. If the gallium content increases, all measured transverse and longitudinal phonon dispersion curves become significantly less rigid (for some of them, the energy almost halved). The authors noted, however, that only a detailed comparison of the results obtained with model calculations based on first principles can provide an understanding of the fundamental mechanisms of the observed effects. New work using these methods is likely nonexistent due to problems with the interpretation of the data obtained in experiments on small-angle and inelastic neutron scattering.

The interpretation of neutron diffraction data is more unambiguous, but they generated several new questions that have not been answered yet, although they seem to be of importance for understanding the processes that occur in Fe–Ga and Fe–Al alloys, including those that are not related to magnetostriction. The main issue is the coherence of the crystal lattices of coexisting disordered and ordered phases in Fe–Ga and Fe–Al, since it involves the general mechanisms of the emergence of equilibrium phase separation. At first glance, this issue has two unrelated aspects. Why does the entire disordered matrix begin to respond to the emergence of clusters of the ordered phase despite the small volume they occupy? Why does the coherence of the lattices of the matrix and clusters occur in the bulk of the sample but is violated in thin layers? The problem of why the entire $D0_3 \rightarrow L1_2$ transition in Fe–Ga alloys cannot be described in the JMAK model is also of interest for further experimental and theoretical studies.

It should be emphasized once again in conclusion that the structural and microstructural information obtained using electron, X-ray, synchrotron, and neutron diffraction is complementary, since none of these methods is universal. This review presents examples of the results obtained by various methods, which may agree with each other or differ significantly. The main reasons for the disagreements are quite apparent: they are primarily associated with a crucial difference between the characteristic thicknesses of the layer of the substance that forms the diffraction pattern and the ensuing specific features of the preparation of samples for a

diffraction experiment in which a particular type of radiation is employed. However, some details still require further analysis.

The experimental data on neutron diffraction discussed in this review were obtained in cooperation with a number of research centers in Russia and other countries with the financial support of the Russian Foundation for Basic Research (project nos 17-52-44024, 18-02-00325, 18-58-52007, and 18-58-53032) and the Russian Science Foundation (project nos 18-12-00283 and 19-72-20080). The authors are grateful to their colleagues from FLNP JINR and MISIS for their fruitful cooperation and joint publications cited in the review. The authors are grateful to the Russian Foundation for Basic Research (Expansiya contest, project no. 19-12-50056) for financial support for writing this review.

References

1. Belov K P et al. *Sov. Phys. Usp.* **26** 518 (1983); *Usp. Fiz. Nauk* **140** 271 (1983)
2. Khachaturyan A G, Viehland D *Metall. Mater. Trans. A* **38** 2308 (2007)
3. Summers E M, Lograsso T A, Wun-Fogle M *J. Mater. Sci.* **42** 9582 (2007)
4. Nagaev E L *Phys. Usp.* **38** 497 (1995); *Usp. Fiz. Nauk* **165** 529 (1995)
5. Aksenov V L, Balagurov A M, Pomyakushin V Yu *Phys. Usp.* **46** 856 (2003); *Usp. Fiz. Nauk* **173** 883 (2003)
6. Golovin I S et al. *Phys. Met. Metallogr.* **121** 851 (2020); *Fiz. Met. Metalloved.* **121** 937 (2020)
7. Wyckoff R W G *Crystal Structures* (New York: John Wiley, 1963)
8. Vonsovskii S V *Magnetism* (New York: J. Wiley, 1974); Translated from Russian: *Magnetizm* (Moscow: Nauka, 1971) pp. 918–925
9. Krinchik G S *Fizika Magnitnykh Yavlenii* (Physics of Magnetic Phenomena) (Moscow: Izd. MGU, 1976) pp. 172–186
10. Kawamiya N, Adachi K, Nakamura Y *J. Phys. Soc. Jpn.* **33** 1318 (1972)
11. Clark A E et al. *IEEE Trans. Magn.* **36** 3238 (2000)
12. Clark A E et al. *J. Appl. Phys.* **93** 8621 (2003)
13. Hall R C *J. Appl. Phys.* **30** 816 (1959)
14. Kubaschewski O *Iron-Binary Phase Diagrams* (Berlin: Springer-Verlag, 1982)
15. Ikeda O et al. *J. Alloys Compd.* **347** 198 (2002)
16. Leineweber A et al. *Intermetallics* **131** 107059 (2021)
17. Vershinina T N et al. *Intermetallics* **131** 107110 (2021)
18. Balagurov A M et al. *J. Appl. Cryst.* **50** 198 (2017)
19. Balagurov A M et al. *Intermetallics* **128** 107016 (2021)
20. Golovin I S et al. *Mater. Lett.* **263** 127257 (2020)
21. Ma T et al. *Nat. Commun.* **8** 13937 (2017)
22. Palacheva V V et al. *Acta Mater.* **130** 229 (2017)
23. Williams D B, Carter C B *Transmission Electron Microscopy. A Textbook for Materials Science* (New York: Plenum Press, 1996)
24. Fetisov G V *Sinkhrotronnoe Izluchenie. Metody Issledovaniya Struktury Veshchestva* (Synchrotron Radiation. Methods of Studying the Structure of Matter) (Moscow: Fizmatlit, 2007)
25. Nozik Yu Z, Ozerov R P, Hennig K *Strukturnaya Neitronografiya* (Structural Neutron Scattering) (Moscow: Atomizdat, 1979)
26. Umanskii Ya S et al. *Kristallografiya, Rentgenografiya i Elektronnaya Mikroskopiya* (Crystallography, X-Ray Scattering, and Electronic Microscopy) (Moscow: Metallurgiya, 1982)
27. Sears V F *Neutron News* **3** 26 (1992)
28. Shull C G, Siegel S *Phys. Rev.* **75** 1008 (1949)
29. Aksenov V L, Balagurov A M *Phys. Usp.* **59** 279 (2016); *Usp. Fiz. Nauk* **186** 293 (2016)
30. Balagurov A M et al. *Phys. Part. Nucl.* **46** 249 (2015); *Fiz. Elem. Chastits Atom. Yadra* **46** 453 (2015)
31. Balagurov A M, Bobrikov I A, Golovin I S *JETP Lett.* **107** 558 (2018); *Pis'ma Zh. Eksp. Teor. Fiz.* **107** 583 (2018)
32. Mittemeijer E J, Welzel U *Z. Kristallogr.* **223** 552 (2008)
33. Wilson A J C *Proc. R. Soc. Lond. A* **181** 360 (1943)
34. Warren B E *X-Ray Diffraction* (Reading, MA: Addison-Wesley Publ. Co., 1969)
35. Iveronova V I, Revkevich G P *Teoriya Rasseyaniya Rentgenovskikh Luchei* (Theory of X-Ray Scattering) (Moscow: Izd. MGU, 1978)
36. Scardi P, in *Powder Diffraction. Theory and Practice* (Eds R F Dinnebier, S J L Billinge) (Cambridge: Royal Society of Chemistry, 2008) pp. 376–413
37. Greenholz M,Kidron A *Acta Cryst. A* **26** 306(1970)
38. Warlimont H, Thomas G *Metal. Sci. J.* **4** 47 (1970)
39. Watanabe D et al. *J. Phys. Soc. Jpn.* **29** 722 (1970)
40. Cullen J R et al. *J. Magn. Magn. Mater.* **226–230** 948 (2001)
41. Wu R *J. Appl. Phys.* **91** 7358 (2002)
42. Lograsso T A et al. *J. Alloys Compd.* **350** 95 (2003)
43. Petrik M V, Gorbatov O I, Gornostyrev Yu N *JETP Lett.* **98** 809 (2013); *Pis'ma Zh. Eksp. Teor. Fiz.* **98** 912 (2013)
44. Petrik M V "Pervoprintsipnye raschety blizhnego poryadka i strukturnogo sostoyaniya v OTsK splavakh zheleza s 3p- i 4p-elementami" ("First-principle calculation of the short order and structural states in bcc alloys of iron with 3p and 4p elements"), PhD Thesis (Phys.-Math. Sci.) (Yekaterinburg: Institute of Metal Physics, Ural Branch of the Russian Academy of Sciences, 2015)
45. Cao H et al. *Phys. Rev. Lett.* **102** 127201 (2009)
46. Du Y et al. *Phys. Rev. B* **81** 054432 (2010)
47. Chernenkov Y P, Ershov N V, Lukshina V A *Phys. Solid State* **61** 1960 (2019); *Fiz. Tverd. Tela* **61** 2000 (2019)
48. Shiiyama K, Ninomiya H, Eguchi T "Evolution of antiphase ordered domain structure and phase separation activated by ordering", in *Research of Pattern Formation* (Ed. R Takaki) (Tokyo: KTK Sci. Publ., 1994) pp. 411–430
49. Ziman J M *Models of Disorder. The Theoretical Physics of Homogeneously Disordered Systems* (Cambridge: Cambridge Univ. Press, 1979); Translated into Russian: *Modeli Besporyadka. Teoreticheskaya Fizika Odnorodno Neuporyadochennykh Sistem* (Moscow: Mir, 1982)
50. Gusev A I *Phys. Usp.* **49** 693 (2006); *Usp. Fiz. Nauk* **176** 717 (2006)
51. Libao L et al. *Physica B* **365** 102 (2005)
52. Xing Q et al. *Acta Mater.* **56** 4536 (2008)
53. He Y et al. *Acta Mater.* **109** 177 (2016)
54. Ke Y et al. *J. Alloys Compd.* **725** 14 (2017)
55. Gou J et al. *Scripta Mater.* **185** 129 (2020)
56. Nie Z et al. *J. Alloys Compd.* **763** 223 (2018)
57. Golovin I S et al. *Intermetallics* **114** 106610 (2019)
58. Balagurov A M et al. *J. Surf. Investig. X-ray, Synchrotron Neutron Tech.* **14** S11 (2020)
59. Matunina M V et al. *Phase Trans.* **92** 101 (2019)
60. Balagurov A M et al. *JETP Lett.* **104** 539 (2016); *Pis'ma Zh. Eksp. Teor. Fiz.* **104** 560 (2016)
61. Balagurov A M et al. *Acta Mater.* **153** 45 (2018)
62. Taylor A, Jones R M *J. Phys. Chem. Solids* **6** 16 (1958)
63. Balagurov A M, Bobrikov I A, Golovin I S *JETP Lett.* **110** 585 (2019); *Pis'ma Zh. Eksp. Teor. Fiz.* **110** 584 (2019)
64. Balagurov A M et al. *Phys. Rev. Mater.* **3** 013608 (2019)
65. Golovin I S et al. *Mater. Des.* **98** 113 (2016)
66. Golovin I S et al. *Intermetallics* **105** 6 (2019)
67. Balagurov A M et al. *Acta Cryst. B* **75** 1024 (2019)
68. Golovin I S et al. *J. Alloys Compd.* **811** 152030 (2019)
69. Li M et al. *J. Alloys Compd.* **701** 768 (2017)
70. Cahn R W *Intermetallics* **7** 1089 (1999)
71. Lograsso T A, Summers E M *Mat. Sci. Eng. A* **416** 240 (2006)
72. Jin T et al. *Intermetallics* **115** 106628 (2019)
73. Cao H et al. *J. Alloys Compd.* **465** 244 (2008)
74. Na S-M, Flatau A B *Proc. SPIE* **5761** 192 (2005)
75. Leineweber A, Mittemeijer E J "Kinetics of phase transformations and of other time-dependent processes in solids analyzed by powder diffraction", in *Modern Diffraction Methods* (Eds E J Mittemeijer, U Welzel) (Singapore: Wiley-VCH, 2013)
76. Kolmogorov A N *Izv. Akad. Nauk SSSR Ser. Matem.* **1** 355 (1937)
77. Johnson W A, Mehl K E *Trans. Am. Inst. Min. Met. Eng.* **195** 416 (1939)
78. Avrami M *J. Chem. Phys.* **9** 177 (1941)
79. Starink M J *J. Mater. Sci.* **32** 4061 (1997)
80. Mudivarthi C et al. *J. Appl. Phys.* **107** 09A957 (2010)
81. Zarestky J L et al. *Phys. Rev. B* **72** 180408(R) (2005)